Geosci. Model Dev. Discuss., 4, 2199–2278, 2011
www.geosci-model-dev-discuss.net/4/2199/2011/
doi:10.5194/gmdd-4-2199-2011

Geoscientific Model Development Discussions

CAM-chem: description and evaluation of interactive atmospheric chemistry in CESM

J.-F. Lamarque[1], L. K. Emmons[1], P. G. Hess[2], D. E. Kinnison[1], S. Tilmes[1], F. Vitt[1], C. L. Heald[3], E. A. Holland[1], P. H. Lauritzen[1], J. Neu[4], J. J. Orlando[1], P. Rasch[5], and G. Tyndall[1]

[1]National Center for Atmospheric Research, Boulder, CO, USA
[2]Cornell University, Ithaca, NY, USA
[3]Colorado State University, Fort Collins, CO, USA
[4]Jet Propulsion Laboratory, Pasadena, CA, USA
[5]Pacific Northwest National Laboratory, Richland, WA, USA

Received: 8 August 2011 – Accepted: 30 August 2011 – Published: 16 September 2011

Correspondence to: J.-F. Lamarque (lamar@ucar.edu)

Published by Copernicus Publications on behalf of the European Geosciences Union.

Abstract

We discuss and evaluate the representation of atmospheric chemistry in the global Community Atmosphere Model (CAM) version 4, the atmospheric component of the Community Earth System Model (CESM). We present a variety of configurations for the representation of tropospheric and stratospheric chemistry, wet removal, and online and offline meteorology. Results from simulations illustrating these configurations are compared with surface, aircraft and satellite observations. Overall, the model indicates a good performance when compared to observations. Major biases include a negative bias in the high-latitude CO distribution and a positive bias in upper-tropospheric/lower-stratospheric ozone, especially when online meteorology is used. The CAM-chem code as described in this paper, along with all the necessary datasets needed to perform the simulations described here, are available for download at http://www.cesm.ucar.edu.

1 Introduction

Atmospheric chemistry plays an integral role in the distribution of the non-CO_2 radiatively active gases and aerosols (Forster et al., 2007). In addition, climate and its evolution strongly influences atmospheric chemistry and air quality (Chen et al., 2009; Jacob and Winner, 2009). Because of the nonlinear behavior of chemistry and the importance of regionally-varying emissions, it is critical to represent the interactions between chemistry and climate using a global three-dimensional model.

We discuss here the representation of atmospheric chemistry (gas phase and aerosol species) in the global Community Atmosphere Model (CAM version 4, Neale et al., 2011), the atmospheric component of the Community Earth System Model (CESM). Due to its full integration in the CESM, CAM-chem provides the flexibility of using the same code to perform climate simulations and simulations with specified meteorological fields. Therefore, CAM-chem can be used in three separate frameworks, all

GMDD
4, 2199–2278, 2011

embedded within CESM: (1) a fully coupled Earth System model (i.e. with all climate components active, which offers the possibility to connect the chemistry with biogeochemical processes in the land and ocean models), (2) with specified sea-surface and sea-ice distributions and (3) with specified meteorological fields. Configurations (1) and (2) are usually referred to as online, while configuration (3) is referred to as offline. In configurations (2) and (3), only the atmosphere and land components of CESM are active. In addition, CAM-chem uses a chemical preprocessor that provides extensive flexibility in the definition of the chemical mechanism, allowing for ease of update and modification.

The availability of a specified dynamics configuration of CAM-chem offers a number of advantages over traditional chemistry-transport models. (1) It allows for consistent simulations between the online and offline versions; (2) It allows the offline version to be run in an Earth System framework so as to fully exploit other model components. In particular it allows an incorporation of the biogeochemical algorithms in the land components; (3) It allows for the radiative algorithms incorporated into CAM4 to be fully exploited in the offline version. This allows a calculation of the radiative forcing within the offline model version, including a calculation of the radiative forcing for specific events (e.g., forest fires) (Pfister et al., 2008; Randerson et al., 2006); (iv) It allows for the strict conservation of tracer mass including accounting for changes in mixing ratio as the water vapor concentration changes within the atmosphere.

Recent applications of CAM-chem have demonstrated its ability to represent tropospheric (Aghedo et al., 2011; Lamarque et al., 2010, 2011a, b) and stratospheric (Lamarque et al., 2008; Lamarque and Solomon, 2010) conditions, including temperature structure and dynamics (Butchart et al., 2010). Offline CAM-chem has been used in the hemispheric transport of air pollution assessments (Fiore et al., 2009; Jonson et al., 2010; Shindell et al., 2008; MacKenzie et al., 2009; Sanderson et al., 2008).

It is the purpose of this paper to document all these aspects of CAM-chem, along with results from associated simulations and their evaluation against observations. The paper is therefore organized as follows: in Sect. 2, we provide a short introduction to

GMDD
4, 2199–2278, 2011

CAM4. In Sect. 3, we discuss all the chemistry-specific parameterizations of CAM-chem. The implementation of the specified-dynamics version is discussed in Sect. 4. Section 5 presents the various chemical mechanisms used in this study. Model simulation setups, including emissions are discussed in Sect. 6, while the comparison to observations is shown in Sect. 7. Discussion and conclusions are in Sect. 8.

2 CAM4 description

The Community Atmosphere Model, version 4 (CAM4, Neale et al., 2011) was released as the atmosphere component of the Community Climate System Model, version 4 (CCSM4) and contains improvements over CAM3 (Collins et al., 2006). In particular, the finite volume dynamical core option available in CAM3 is now the default primarily due to its superior tracer transport properties (Rasch et al., 2006). As in CAM3, deep convection is parameterized using the Zhang-McFarlane approach (1995), but with modifications as discussed below, while shallow convection follows Hack et al. (2006). Additional information on the representation of clouds and precipitation processes can be found in Boville et al. (2006). Finally, processes in the planetary boundary layer are represented using the Holtslag and Boville (1993) parameterization.

Changes made to the representation of deep convection include a dilute plume calculation and the introduction of Convective Momentum Transport (CMT). In addition, the cloud fraction has an additional calculation to improve thermodynamic consistency. A freeze-drying modification is further made to the cloud fraction calculation in very dry environments, such as Arctic winter, where cloud fraction and cloud water estimates were somewhat inconsistent in CAM3.

Altogether, only marginal improvements over CAM3 are found in the large-scale aspects of the simulated climate (see Neale et al., 2011 for a complete description of the model performance). Indeed, it is found that the implementation of the finite volume dynamical core leads to a degradation in the excessive trade-wind simulation, but with an accompanying reduction in zonal stresses at higher latitudes. But, CMT reduces much

GMDD
4, 2199–2278, 2011

of the excessive trade-wind biases. Plume dilution leads to a moister deep tropics alleviating much of the mid-tropospheric dry biases and reduces the persistent precipitation biases over the Arabian peninsula and the southern Indian ocean associated with the Indian Monsoon. Finally, the freeze-drying modification alleviates much of the wintertime excessive cloud bias and improves the associated surface cloud-related energy budget.

3 Chemistry-specific parameterizations

CAM-chem borrows heavily from MOZART-4 (Emmons et al., 2010, referenced hereafter as E2010). In particular, many of the parameterizations needed to represent atmospheric chemistry in a global model are adapted or expanded from their equivalents in MOZART-4. However, for completeness, we will include a brief description of those parameterizations (and their updates, whenever applicable).

3.1 Dry deposition

Dry deposition is represented following the resistance approach originally described in Wesely (1989); as discussed in E2010, this earlier paper was subsequently updated and we have included all updates (Walcek et al., 1986; Walmsley and Wesely, 1996; Wesely and Hicks, 2000). Following this approach, all deposited chemical species (the specific list of deposited species is defined along with the chemical mechanisms, see Sect. 4) are mapped to a weighted-combination of ozone and sulfur dioxide depositions; this combination represents a definition of the ability of each considered species to oxidize or to be taken up by water. In particular, the latter is dependent on the effective Henry's law coefficient. While this weighting is applicable to many species, we have included specific representations for CO/H_2 (Yonemura et al., 2000; Sanderson et al., 2003), and peroxyacetylnitrate (PAN, Sparks et al., 2003). Furthermore, it is assumed that the surface resistance for SO_2 can be neglected (Walcek et al., 1986).

GMDD
4, 2199–2278, 2011

Finally, following Cooke et al. (1999), the deposition velocities of black and organic carbonaceous aerosols are specified to be 0.1 cm s^{-1} over all surfaces. Dust and sea-salt are represented following Mahowald et al. (2006a, b).

The computation of deposition velocities in CAM-chem takes advantage of its coupling to the Community Land Model (CLM; http://www.cesm.ucar.edu/models/cesm1.0/clm/index.shtml). In particular, the computation of surface resistances in CLM leads to a representation at the level of each plant functional type (Table 1) of the various drivers for deposition velocities. The grid-averaged velocity is computed as the weighted-mean over all land cover types available at each grid point. This ensures that the impact on deposition velocities from changes in land cover, land use or climate is taken into account.

In addition, the same dry deposition approach is separately applied to water surfaces i.e., lakes and oceans, including sea-ice. It is then combined with the land-based value, weighted by the ocean/sea-ice and land fractions in each model grid cell.

3.2 Biogenic emissions

Similar to the treatment of dry deposition over land, biogenic emissions of volatile organic compounds (isoprene and monoterpenes) are calculated based upon the land cover. These are made available for atmospheric chemistry, unless the user decides to explicitly set those emissions using pre-defined (i.e. contained in a file) gridded values. Details of this implementation in the CLM3 are discussed in Heald et al. (2008); we provide a brief overview here.

Vegetation in the CLM model is described by 17 plant function types (PFTs, see Table 1). Present-day land surface parameters such as leaf area index are consistent with MODIS land surface data sets (Lawrence and Chase, 2007). Alternate land cover and density can be either specified or interactively simulated with the dynamic vegetation model of the CLM for any time period of interest.

Isoprene emissions follow the MEGAN2 (Guenther et al., 2006) algorithms for a detailed canopy model (CLM). This includes mapped PFT-specific emission factors to

GMDD
4, 2199–2278, 2011

account for species divergent emissions of isoprene. These standard emission factors are modulated by activity factors accounting for the effect of temperature, radiation, leaf age, vegetation density (LAI) and soil moisture. Seasonal maps are shown in the supplement, Fig. S1; annual totals are approximately 500 Tg yr^{-1}.

Total monoterpene emissions follow the earlier work of Guenther et al. (1995) as implemented in the CLM by Levis et al. (2003). Baseline emission factors are specified for each plant function type and are scaled by an exponential function of leaf temperature.

3.3 Wet deposition

Wet removal of soluble gas-phase species is the combination of two processes: in-cloud, or nucleation scavenging (rainout), which is the local uptake of soluble gases and aerosols by the formation of initial cloud droplets and their conversion to precipitation, and below-cloud, or impaction scavenging (washout), which is the collection of soluble species from the interstitial air by falling droplets or from the liquid phase via accretion processes (e.g. Rotstayn and Lohmann, 2002). Removal is modeled as a simple first-order loss process $X_{iscav} = X_i \cdot F \cdot (1 - \exp(-\lambda\ \Delta t))$. In this formula, X_{iscav} is the species mass (in kg) and X_i scavenged in time step Δt, F is the fraction of the grid box from which tracer is being removed, and λ is the loss rate. In-cloud scavenging is proportional to the amount of condensate converted to precipitation, and the loss rate depends on the amount of cloud water, the rate of precipitation formation, and the rate of tracer uptake by the liquid phase. Below-cloud scavenging is proportional to the precipitation flux in each layer and the loss rate depends on the precipitation rate and either the rate of tracer uptake by the liquid phase (for accretion processes), the mass-transfer rate (for highly soluble gases and small aerosols), or the collision rate (for larger aerosols). In CAM-chem two separate parameterizations are available: Horowitz et al. (2003) from MOZART-2 and Neu and Prather (2011).

The distinguishing features of the Neu and Prather scheme are related to three aspects of the parameterization: (1) the partitioning between in-cloud and below cloud scavenging, (2) the treatment of soluble gas uptake by ice and (3) the Neu and Prather

GMDD
4, 2199–2278, 2011

scheme uniquely accounts for the spatial distribution of clouds in a column and the overlap of condensate and precipitation. Given a cloud fraction and precipitation rate in each layer, the scheme determines the fraction of the gridbox exposed to precipitation from above and that exposed to new precipitation formation under the assumption of maximum overlap of the precipitating fraction. Each model level is partitioned into as many as four sections, each with a gridbox fraction, precipitation rate, and precipitation diameter: (1) Cloudy with precipitation falling through from above; (2) Cloudy with no precipitation falling through from above; (3) Clear sky with precipitation falling through from above; (4) Clear sky with no precipitation falling from above. Any new precipitation formation is spread evenly between the cloudy fractions (1 and 2). In region 3, we assume a constant rate of evaporation that reduces both the precipitation area and amount so that the rain rate remains constant. Between levels, we average the properties of the precipitation and retain only two categories, precipitation falling into cloud and precipitation falling into ambient air, at the top boundary of each level. If the precipitation rate drops to zero, we assume full evaporation and random overlap with any precipitating levels below. Our partitioning of each level and overlap assumptions are in many ways similar to those used for the moist physics in the ECMWF model (Jakob and Klein, 2000).

The transfer of soluble gases into liquid condensate is calculated using Henry's Law, assuming equilibrium between the gas and liquid phase. Nucleation scavenging by ice, however, is treated as a burial process in which trace gas species deposit on the surface along with water vapor and are buried as the ice crystal grows. Kärcher and Voigt (2006) have found that the burial model successfully reproduces the molar ratio of HNO_3 to H_2O on ice crystals as a function of temperature for a large number of aircraft campaigns spanning a wide variety of meteorological conditions. We use the empirical relationship between the HNO_3:H_2O molar ratio and temperature given by Karcher and Voigt (2006) to determine in-cloud scavenging during ice particle formation, which is applied to nitric acid only. Below-cloud scavenging by ice is calculated using a rough representation of the riming process modeled as a collision-limited first

GMDD
4, 2199–2278, 2011

order loss process. Neu and Prather (2011) provide a full description of the scavenging algorithm.

On the other hand, the Horowitz approach uses the rain generation diagnostics from the large-scale and convection precipitation parameterizations in CAM; equilibrium between gas-phase and liquid phase is then assumed based on the effective Henry's law.

3.4 Lightning

The emissions of NO from lightning are included as in E2010, i.e. using the Price parameterization (Price and Rind, 1992; Price et al., 1997), scaled to provide a global annual emission of 3–4 Tg(N) yr^{-1}. The vertical distribution follows DeCaria et al. (2006) as in E2010. In addition, the strength of intra-cloud (IC) lightning strikes is assumed to be equal to cloud-to-ground strikes, as recommended by Ridley et al. (2005).

3.5 Polar stratospheric clouds and associated ozone depletion

The representation of polar stratospheric clouds follows exactly the approach in the Whole Atmosphere Chemistry Climate Model (Kinnison et al., 2011). It is therefore an update over the version used in all the CCMval-2 analysis papers (e.g. Austin et al., 2010) in which it was shown that CAM-chem (identified in those studies as CAM3.5) was underestimating the extent and depth of Antarctic ozone hole depletion. In particular, as in WACCM4, we are now using a strict enforcement of the conservation of total chlorine and total bromine under advection. Indeed, it has been identified that the existence of strong gradients in the stratosphere led to non-conservation issues of the total bromine and chlorine, as computed from the sum of their components, related to inaccuracies in transport algorithms. We are therefore forcing the conservation through the addition of two additional tracers: TCly and TBry. These tracers are specified at the lower boundary and reflect the total amount of Br and Cl atoms in the atmosphere following the observed concentrations of all considered halogen species in the model.

GMDD
4, 2199–2278, 2011

In addition, we have updated the heterogeneous chemistry module to reflect that the model was underestimating the supercooled ternary solution (STS) surface area density (SAD). The previous version (used in the CCMval-2 simulations and described in Kinnison et al., 2007) allowed the available HNO_3 to first form nitric acid trihydrate (NAT); then the resulting gas-phase HNO_3 was available to form STS SAD. In the new version the approach is reversed, with the available HNO_3 to first form STS aerosol. This enhances the STS SAD that is used to derive heterogeneous conversion of reservoir species to more active, odd-oxygen depleting species. Observational studies have shown that STS is the main PSC for odd-oxygen loss and therefore this is a better representation of stratospheric heterogeneous processes (e.g., Lowe and MacKenzie, 2008). After formation of STS aerosol, there is still enough gas-phase HNO_3 available to form NAT. The effective radius of NAT is then used to settle the condensed phase HNO_3 and eventual irreversible denitrification occurs. The updated heterogeneous module and its performance are discussed in detail in Kinnison et al. (2011).

3.6 Photolysis

In CAM-chem, only the lookup table approach from MOZART-3 (Kinnison et al., 2007) is available at this time. As an extension of MOZART-4 and to provide the ability to seamlessly perform tropospheric and stratospheric chemistry simulations, we have included the calculation of photolysis rates for wavelengths shorter than 200 nm; this was shown to be important for ozone chemistry in the tropical upper troposphere (Prather, 2009). In addition, because the standard configuration of CAM only extends into the lower stratosphere (model top is usually around 40 km), we have included an additional layer of ozone and oxygen above the model top to provide a very accurate representation of photolysis rates in the upper portion of the model (Fig. 1) as compared to the equivalent calculation using a fully-resolved stratospheric distribution. The fully resolved stratospheric module was evaluated in Chapter 6 of the SPARC CCMVal report on the Evaluation of Chemistry-Climate Models. This photolysis module was shown to be one of the more accurate modules used in CCMs (see SPARC, 2010 for details).

GMDD
4, 2199–2278, 2011

While the lookup table provides explicit quantum yields and cross-sections for a large number of photolysis rate determinations, additional ones are available by scaling of any of the explicitly defined rates. This process is available in the definition of the chemical preprocessor input files (see Sect. 3 for a complete list of the photolysis rates available).

The impact of clouds on photolysis rates is parameterized following Madronich (1987). However, because we use a lookup table approach, the impact of aerosols (tropospheric or stratospheric) on photolysis rates cannot be represented.

4 Offline meteorology

We have incorporated in CAM-chem the capability to perform simulations using specified dynamics, where offline meteorological fields are input into the model instead of calculated online. This procedure can allow for more precise comparisons between measurements of atmospheric composition and model output. To allow for simulations using input meteorological fields we follow the same procedure as used originally in the Model of Atmospheric Transport and Chemistry (MATCH) (Rasch et al., 1997) and subsequently used in all versions of MOZART (E2010; Kinnison et al., 2007, Horowitz et al., 2003; Brasseur et al., 1998). In this procedure only the horizontal wind components, air temperature, surface temperature, surface pressure, sensible and latent heat flux and wind stress (see Table 2) are read into the model simulation from the input meteorological dataset. These fields are subsequently used to internally generate (using the existing CAM4 parameterizations) the variables necessary for (1) calculating subgrid scale transport including boundary layer transport and convective transport; (2) the variables necessary for specifying the hydrological cycle, including cloud and water vapor distributions and rainfall (see Rasch et al., 2007 for more details).

After the meteorological fields are read into CAM-chem from the offline meteorological dataset, CAM-chem updates these meteorological fields in conjunction with the

GMDD
4, 2199–2278, 2011

variables describing atmospheric composition for use in the next timestep. CAM-chem uses a sub-stepping procedure to solve the advection equations for the mass flux, temperature and velocity fields over each timestep. As in the online version of the model these fields are allowed to evolve over each substep. We have found that this evolution dampens some of the inconsistencies between the inserted and model-computed velocity and mass fields subsequently used for tracer transport. The mass flux at each sub-step is accumulated to produce the net mass flux over the entire time step. A graphical explanation of the sub-cycling is given in Lauritzen et al. (2011).

In addition, a mass fixer algorithm is necessary as the mass flux computed from the offline meteorological winds input into CAM4 will not in general produce a mass distribution consistent with the offline surface pressure field. If uncorrected this may lead to spurious changes in tracer mass, concentration or surface pressure (Rotman et al., 2004). The mass fixer algorithm ensures that the calculated surface pressure closely matches the surface pressure in the offline meteorological dataset (see discussion in Rotman et al., 2004). The mass fixer algorithm makes the appropriate adjustments to the horizontal mass fluxes to produce a resulting mass distribution consistent with the evolution of surface pressure in the input meteorological dataset. The procedure follows the algorithm given in Rotman et al. (2004): first it uses an efficient algorithm to find the correction to the vertically integrated mass flux, then the corrected mass flux is distributed in the vertical in proportion to the dependence of each model level on the surface pressure in a hybrid coordinate system. The edge pressures of the Lagrangian mass surfaces are consistently adjusted to allow for the vertical remapping of the transported fields to the fixed hybrid pressure coordinate system. Following the corrections in mass flux and the edge pressures the constituent tracers are transported by the large-scale wind fields.

Currently, we recommend for input offline meteorology the NASA Goddard Global Modeling and Assimilation Office (GMAO) GEOS-5 generated meteorology. Using this meteorological dataset and the formulation of offline CAM-chem as described above, multi-year simulations (see Sect. 5) do not seem to require the use of limiters

GMDD
4, 2199–2278, 2011

of stratosphere-troposphere exchange such as SYNOZ (McLinden et al., 2000). All GEOS-5 meteorological datasets, including the Modern Era Retrospective-Analysis For Research And Applications (MERRA) datasets, are available at the standard CAM resolution of 1.9°×2.5° on the Earth System Grid (http://www.earthsystemgrid.org/home.htm). These files were generated from the original resolution by using a conservative regridding procedure based on the same 1-D operators as used in the transport scheme of the finite-volume dynamical core used in GEOS-5 and CAM (S.-J. Lin, personal communication, 2009). Note that because of a difference in the sign convention of the surface wind stress (TAUX and TAUY) between CESM and GEOS5/MERRA, these fields in the interpolated datasets have been reversed from the original files supplied by GMAO. In addition, it is important for users to recognize the importance of specifying the correct surface geopotential height (PHIS) to ensure consistency with the input dynamical fields, which is important to prevent unrealistic vertical mixing.

5 Chemical mechanisms

As mentioned in the Introduction, CAM-chem uses the same chemical preprocessor as MOZART-4. This preprocessor generates Fortran code for each specific chemical mechanism, allowing for an easy update and modification of existing chemical mechanisms. In particular, the generated code provides two chemical solvers, one explicit and one semi-implicit, which the user specifies based on the chemical lifetime of each species.

We provide in this paper two chemical mechanisms, (1) extensive tropospheric chemistry, and (2) extensive tropospheric and stratospheric chemistry. All species and reactions are listed in Tables 3 and 4, respectively. In both mechanisms described in this paper, CAM-chem uses the bulk aerosol model discussed in Lamarque et al. (2005) and E2010. This model has a representation of aerosols based on the work by Tie et al. (2001, 2005), i.e. sulfate aerosol is formed by the oxidation of SO_2 in the gas phase (by reaction with the hydroxyl radical) and in the aqueous phase (by reaction

GMDD
4, 2199–2278, 2011

with ozone and hydrogen peroxide). Furthermore, the model includes a representation of ammonium nitrate that is dependent on the amount of sulfate present in the air mass following the parameterization of gas/aerosol partitioning by Metzger et al. (2002). Because only the bulk mass is calculated, a lognormal distribution (Table 5, also see E2010) is assumed for all aerosols using different mean radius and geometric standard deviation (Liao et al., 2003). The conversion of carbonaceous aerosols (organic and black) from hydrophobic to hydrophilic is assumed to occur within a fixed 1.6 days (Tie et al., 2005). Natural aerosols (desert dust and sea salt) are implemented following Mahowald, et al. (2006a, b), and the sources of these aerosols are derived based on the model calculated wind speed and surface conditions. In addition, secondary-organic aerosols (SOA) are linked to the gas-phase chemistry through the oxidation of atmospheric non-methane hydrocarbons (NMHCs) as in Lack et al. (2004).

The extensive tropospheric chemistry scheme represents a minor update to the MOZART-4 mechanism, fully described in E2010. In particular, we have included C_2H_2, HCOOH, HCN and CH_3CN. Reaction rates have been updated to JPL-2006 (Sander et al., 2006). A minor update has been made to the isoprene oxidation scheme, including an increase in the production of glyoxal. This mechanism is mainly of relevance in the troposphere and is intended for simulations for which long-term trends in the stratospheric composition are not crucial. Therefore, in this configuration, the stratospheric distributions of long-lived species (see discussion below) are specified from previously performed WACCM simulations (Garcia et al., 2007; see Sect. 6.3).

On the other hand, in the case where changes in stratospheric composition are important, for which the dynamics is calculated online, we have added a stratospheric portion to the tropospheric chemistry mechanism described above. This addition (of species and reactions, see Tables 3 and 4) is taken from the WACCM mechanism as this has been shown to perform very well in the recent CCMval-2 analysis (SPARC, 2010). The overall description of this chemistry is discussed in Kinnison et al. (2011) and includes updates to JPL-2006 (Sander et al., 2006).

GMDD
4, 2199–2278, 2011

6 Simulations setup, including emissions and other boundary conditions

All simulations discussed in this paper are performed at the horizontal resolution of 1.9° (latitude) and 2.5° (longitude). The number of vertical levels ranges from 26 levels (online dynamics) to 56 levels (GEOS-5 and MERRA meteorology); in both cases, the model extends to approximately 3 hPa (≈40 km). The online simulation is performed using the Neu removal scheme, while the specified dynamics simulations are performed using the MOZART wet removal scheme. A summary is provided in Table 6.

6.1 Emissions

Available with the distribution of the CAM-chem, we are providing emissions for tropospheric chemistry that are an extension of the datasets discussed in E2010, covering 1992–2010. More specifically, for 1992–1996, which is prior to satellite-based fire inventories, monthly mean averages of the fire emissions for 1997–2008 from GFED2 (van der Werf et al., 2006 and updates) are used for each year. For 2009–2010, fire emissions are from FINN (Fire INventory from NCAR) (Wiedinmyer et al., 2010). As discussed in E2010, most of the anthropogenic emissions come from the POET (Precursors of Ozone and their Effects in the Troposphere) database for 2000 (Granier et al., 2005). The anthropogenic emissions (from fossil fuel and biofuel combustion) of black and organic carbon determined for 1996 are from Bond et al. (2004). For SO_2 and NH_3, anthropogenic emissions are from the EDGAR-FT2000 and EDGAR-2 databases, respectively (http://www.mnp.nl/edgar/). For Asia, these inventories have been replaced by the Regional Emission inventory for Asia (REAS) with the corresponding annual inventory for each year simulated (Ohara et al., 2007). Aircraft emissions have global annual totals of 0.63 Tg yr^{-1} (1.35 TgN yr^{-1}) for NO, 1.70 Tg yr^{-1} for CO and 0.16 Tg yr^{-1} for SO_2. Only the Asian emissions from REAS vary each year, all other emissions are repeated annually for each year of simulation. The DMS emissions are monthly means from the marine biogeochemistry model HAMOCC5, representative of the year 2000 (Kloster et al., 2006). SO_2 emissions from continuously

GMDD
4, 2199–2278, 2011

outgassing volcanoes are from the GEIAv1 inventory (Andres and Kasgnoc, 1998). Totals for each year and emitted species are listed in Table 7.

Note that while the emissions are provided at the model resolution, any emissions resolution can be used and the model automatically interpolates to the model resolution. At this point, this interpolation is however a simple linear interpolation and therefore does not ensure exact conservation of emissions between resolutions.

6.2 Lower boundary conditions

For all long-lived species (see Table 3), the surface concentrations (Fig. 2) are specified using the historical reconstruction from Meinshausen et al. (2011). In addition, for CO_2 and CH_4, an observationally-based seasonal cycle and latitudinal gradient are imposed on the annual average values provided by Meinshausen et al. (2011). These values are used in the model by overwriting at each time step the corresponding model mixing ratio in the lowest model level with the time (and latitude, if applicable) interpolated specified mixing ratio.

6.3 Specified stratospheric distributions

In the case where no stratospheric chemistry is explicitly represented in the model, it is necessary to ensure a proper distribution of some chemically-active stratospheric (namely O_3, NO, NO_2, HNO_3, CO, CH_4, N_2O, and N_2O_5) species, as is the case for MOZART-4. This monthly-mean climatological distribution is obtained from WACCM simulations covering 1950–2005 (Garcia et al., 2007). Because of the vast changes that occur over that time period, our data distribution provides files for three separate periods: 1950–1959, 1980–1989 and 1996–2005. This ensure that users can perform simulations with a stratospheric climatology representative of the pre-CFC era, as well as during the high CFC and post-Pinatubo era. Not that additional datasets can easily be constructed if necessary.

GMDD
4, 2199–2278, 2011

7 Comparison with observations

The purpose of this section is to document the model chemistry performance against observations for the 3 model setups described in Sect. 6 (see Table 6 for a summary). The model performance for simulating climate and meteorological features is thoroughly discussed in Lamarque et al. (2008), Lamarque and Solomon (2010) and in Neale et al. (2011) and is therefore not presented here. The comparison will make use of a variety of measurements: surface, airborne and satellite. In the case of the online stratosphere-troposphere version, the comparison will include evaluation of modeled stratospheric distributions.

7.1 Comparison with ozonesondes

Due to its central role in tropospheric chemistry and the availability of numerous ozone sonde measurements dating several decades (Logan, 1994), we focus our first evaluation on tropospheric ozone use ozone sonde measurements averaged of representative regions (supplement Fig. S2; Tilmes et al., 2011). For a variety of sites spanning the whole globe (especially in the meridional direction), the data coverage allows the comparison of profiles (Fig. 3), seasonal cycles (Fig. 4) and long-term changes (Fig. 5).

In many of the high-latitude Northern Hemisphere stations (Fig. 3), the model seems to provide a position of the tropopause that is lower than observed, leading to an overestimate of the ozone mixing ratio in the lower stratosphere (i.e. 200–300 hPa). While all simulations use the same emissions, the GEOS-5 version of the model seems to perform the best over those regions. On the other hand, the online simulation leads to a positive bias in the troposphere; it is likely that this is due to a misrepresentation of transport, and more specifically stratosphere-troposphere exchange, in CAM. Overall, the Northern Hemisphere seems to be biased slightly high in the model. However, profiles in the tropical regions and Southern Hemisphere are very well reproduced by all versions of the model.

GMDD
4, 2199–2278, 2011

The seasonal cycle comparison (Fig. 4) indicates that the GEOS5 meteorology provides on average the best fit. The varying degrees of time lag between the model results and the observations in the mid-troposphere seems to indicate that the strength of the coupling between the upper and middle-troposphere is somewhat different between the various dynamical fields.

Over much of the Northern Hemisphere mid-latitudes and poleward, annual-mean biases in the upper-troposphere (250 hPa) are on the order of 25–50 ppbv, especially true in the spring. These biases are lower (5–10 ppbv) in the mid-troposphere (500 hPa). In the surface layer, the model bias tends to peak in the spring in the higher latitudes, especially in the MERRA-driven simulation (probably due to more mixing of stratospheric air).

Many of the differences between model simulations and observations in the Southern Hemisphere Polar regions lower troposphere are present in all versions, indicating that this is likely related to issues in emissions or chemistry. Except for a low bias in the 250 hPa values of the same region, the rest of the Southern Hemisphere ozone distribution is quite well reproduced by all model versions, with smaller biases than in the Northern Hemisphere.

The analysis of long-term changes (Fig. 5) indicates that observed meteorology is important in representing interannual variability, especially in the upper troposphere. Nevertheless, key features (peak amplitude and season) of the variability of mid-troposphere ozone in the Northern Hemisphere seem to be better captured by the online simulation, indicating the positive role of consistently representing transport and chemistry. While the analyzed period is too short for trend analysis, the lower troposphere evolution at Edmonton seems in agreement with the model-underestimated surface ozone trends discussed in Lamarque et al. (2010), even though those latter simulations were performed with different emissions and a different chemical mechanism.

The annual budget for tropospheric ozone is summarized in Table 8; note that these are averaged numbers, with an interannual variability on the order of 10 %. We find that

GMDD
4, 2199–2278, 2011

the online and offline versions have similar tropospheric (defined here as the region of the atmosphere where the ozone mixing ratio is lower than 100 ppbv) burdens and depositions, but with an overall smaller net ozone production in the case of the offline meteorology. The corollary to this comparison is that the diagnosed stratosphere-troposphere flux of ozone (computed as the difference between the deposition and net chemical production) ranges from 410 Tg yr^{-1} (online) to 520 Tg yr^{-1} (offline), within the range of published estimates (e.g. 515–550 Tg yr^{-1}, Hsu et al., 2005; 556±154 Tg yr^{-1}, Stevenson et al., 2005). In the case of the online simulation, this leads to an ozone lifetime of ≈25 days, in excellent agreement with Stevenson et al. (2005).

7.2 Comparison with aircraft observations

As a standard benchmark evaluation, we have performed comparison with the aircraft observations in the Emmons et al. (2000) climatology (Fig. S3 in the supplement). In particular, these plots were used to assess that the Neu and Prather wet removal scheme behaves similarly to the Horowitz scheme. In this section, we focus on specific campaigns targeting the Northern Hemisphere, since this is the region where some of the largest surface ozone biases were found. Therefore, we limit our analysis (Fig. 6) to the INTEX-A (Singh et al., 2007) and INTEX-B (Singh et al., 2009) campaigns. We only use the offline (MERRA and GEOS-5) simulations, as comparison to campaign data is most meaningful with simulations using realistic meteorology. Note that the model contains a procedure to output all specified variables at the time (within the limits of the model timestep, in this case 30 min) and location (or vicinity) of the aircraft observations.

During INTEX-A (Central and Eastern United States, Fig. 6a, b), we find that the model provides a very good representation of the free troposphere, with a negative bias in the mid-troposphere light hydrocarbons, probably due to inaccurate emission ratios (E2010). However, it is clear that the model overestimates surface ozone; this was noted and discussed in Lin et al. (2008) and is likely associated with a misrepresentation in the model of boundary-layer and surface processes, in addition to the coarse

GMDD
4, 2199–2278, 2011

horizontal resolution (Wild and Prather, 2006). Additionally, lowermost troposphere mixing ratios are overestimated, such as hydrogen peroxide and peroxyacetyl nitrates. It is also interesting to note the underestimate of nitrogen oxides in the upper troposphere; this is true in both regions and is possibly related to an underestimate of lightning emissions in the upper troposphere. Indeed, additional analysis of Alaska and Hawaii (see below) do not display such discrepancies.

During INTEX-B Alaska flights (Fig. 6c, d), the model is showing a good agreement with many species, except for the same bias in CO, HCN, ethane and propane noted before. Similar agreements are found for the Hawaii flights (Fig. 7d) except for a slight overestimate of nitric acid in the lower troposphere.

In addition, Fig. 6 contains the distribution as computed in MOZART-4 (E2010) simulations using the same chemistry, meteorology and emissions as the respective GEOS and MERRA simulations with CAM-chem. For most species, we find an overall agreement between the two models, as could be expected from such similar models. There is however the indication that CAM-chem has a slightly larger OH distribution, as indicated by the lower vertical profiles of CO, HCN, C_2H_6 and C_3H_8. The computed tropospheric lifetime of CO is almost exactly the same between the various versions tested here, with values ranging between 1.5 and 1.7 months, very similar to the results from Horowitz et al. (2003). In addition, our tropospheric methane lifetime (reaction with OH only) is on the order of 9.3 years, similar to E2010, Shindell et al. (2006) and Horowitz et al. (2003), indicating that CAM-chem behaves very similarly to the MOZART-2 and MOZART-4 models. Also, it is interesting to note that MOZART-4 has a slightly lower bias in surface ozone, indicating that the differences between the models with respect to physics parameterizations might have led to a slight deterioration of this quantity. Since the main difference (see Sect. 2) appears to be in the representation of deep convection, this bias might be an indication that the boundary-layer is less ventilated than previous versions. More analysis is required to fully assess these differences.

GMDD
4, 2199–2278, 2011

7.3 Comparison with surface carbon monoxide

Surface mixing ratio of carbon monoxide represents one of longest records of tropospheric composition; for this comparison we use all years available from the National Oceanic and Atmospheric Administration data (available at http://www.esrl.noaa.gov/gmd/ccgg/iadv/, e.g. Novelli et al., 2003). Furthermore, because of its strong link to the hydroxyl radical OH, the overall concentration and seasonal cycle of CO is an important indicator of the representation of the tropospheric oxidative capacity (Lawrence et al., 2001). For that purpose, we compare the model results (in this case the online and MERRA simulations, in order to have a sufficiently long record) in terms of the latitudinal distribution of the annual mean and seasonal cycle (Fig. 7a, b, respectively).

Overall, the model accurately represents the latitudinal distribution of CO (strongly driven by gradients in emissions); it also represents the Southern Hemisphere annual mean, but underestimates the high-latitude Northern Hemisphere values, similar to the multi-model results in Shindell et al. (2006). This is further confirmed by the comparison to the retrieved CO columns by the Measurements of Pollution in The Troposphere (MOPITT v4, Deeter et al., 2010, supplement Fig. S4). The average bias against surface observations is 2.8 ppb for the MERRA simulation and −8.3 ppb for the online simulation.

Similarly, the seasonal cycle is quite well represented over all the latitudes, expect in the Polar Northern Hemisphere. This is in agreement with an estimated CO tropospheric lifetime (with respect to OH loss) of approximately 1.5 months, in all simulations, as mentioned above. We have also compared (see supplement, Fig. S5) our tropospheric OH distribution with the Spivakovsky climatology (Spivakovsky et al., 2000) using the Lawrence et al. (2001) diagnostic approach. In that case, we find that our OH distribution is in quite good agreement. It is however smaller (20–30%) in the tropical mid-troposphere, especially in the Southern Hemisphere; it is also larger in the Northern mid-latitudes, except in the mid-troposphere. Based on this analysis, the closest OH distribution to Spivakosky's is provided by the GEOS-5 simulation.

GMDD
4, 2199–2278, 2011

7.4 Comparison with total ozone column

The availability of stratospheric chemistry in the online simulation warrants the comparison with the satellite observed total ozone column. In particular, we use here the gridded EP-TOMS and OMI-TOMS (available at http://toms.gsfc.nasa.gov). The data are zonally- and monthly-averaged before comparison with the model field (Fig. 8). The overall features (latitudinal distribution and seasonal cycle, including the Antarctic ozone hole) and interannual variability are well reproduced. In particular, even though the model has a limited vertical extension and resolution in the stratosphere, the tropical ozone column is rather quite well reproduced.

To further compare with observed values, we focus (Fig. 9) on comparing the long-term variability in high-latitude spring ozone (March in the Northern Hemisphere and October in the Southern Hemisphere). Because the online model is only driven by the observed sea-surface temperatures, there is no expectation that a single-year in the model simulation will be directly comparable with observations; instead, only the mean and standard deviation are relevant in this case. Figure 9 shows that, unlike the version used in the CCMVal-2 simulations (Austin et al., 2010), this updated version has a good representation of the ozone hole (mean and interannual variability), with a limited underestimate (mean bias is −6.8 DU not considering the highly unusual 2002 conditions) of the mean October Antarctic ozone hole. Similarly the mean Northern Hemisphere March ozone distribution is slightly negatively biased (mean bias is −4.9 DU). Note however that the model is not quite able to reproduce the Northern Hemisphere dynamical interannual variability due to its limited representation of the stratosphere (Morgenstern et al., 2010).

7.5 Comparison with stratospheric observations

Because we have significantly modified the representation of stratospheric chemistry processes, we are including here comparisons with the Grooß and Russell climatology (2005), along with recently available ACE-FTS (ACE: Atmospheric Chemistry

GMDD
4, 2199–2278, 2011

Experiment Fourier Transform Spectrometer) measurements (Figs. 10 and 11). ACE is a Canadian-led instrument on the SCISAT satellite (Bernath et al., 2005; Cooper et al., 2011); it measures solar occultation infrared spectra with high-spectral resolution. Stratospheric ozone retrievals agree with ozonesondes within 10 % (Cooper et al., 2010).The climatology from Grooß and Russell uses observations between 1991 and 2004. ACE observations were averaged over a period between 2004 and 2010. Averages of ACE data we derived from the data within the 5h and 95th percentile, to filter for unrealistic large mixing ratios in the data set.

In addition to the reasonable total ozone column, we find that the stratosphere-troposphere model provides a very realistic representation of stratospheric composition, especially in the lower stratosphere, similar to the CAM3.5 results presented in Lamarque et al. (2008); this is particularly true considering the difference between the two observational datasets and different observational periods. It is however clear that the limited vertical extent of the model (approx. 40 km) restricts the chemistry (and photolysis in particular) to regions below some of the main loss regions; this is especially true for long-lived species such as methane (e.g., see 46 hPa extratropical values) and to some extent for the amount of nitric acid available for heterogeneous chemistry.

7.6 Comparison with aerosol observations

Owing to the availability of a large set of observations (time and speciation), we focus our analysis on the Interagency Monitoring of Protected Visual Environments (IMPROVE, Malm et al., 2004) dataset (available for download at http://vista.cira.colostate.edu/IMPROVE/Data/data.htm). We perform a comparison of sulfate, elemental carbon, organic carbon (including secondary organic aerosols, SOA) and ammonium nitrate.

We first present correlations (Fig. 12) between long-term mean (1998–2009) observations and model results (interpolated to the location of the observing stations); note that the IMPROVE sites are located in remote locations (such as National Parks) and are therefore representative of the rural environment, not urban. We find, as presented in other analyses of the behavior of the bulk-aerosol model discussed here

GMDD
4, 2199–2278, 2011

(Lamarque et al., 2011b) that sulfate is quite well represented by the model, however slightly positively biased. On the other hand, both elemental and organic carbon aerosols are underestimated in the model, especially for the sites with medium to high concentrations. Somewhat surprisingly, owing to the inherent difficulties in representing ammonium nitrate in a model and to the fairly simple representation of its formation in the model, we find that ammonium nitrate is quite reasonable, albeit underestimated for the sites with high concentrations.

To further document the behavior of the bulk-aerosol scheme over the United States, we present in Fig. 13 the probability density function of the mean annual and seasonal (summer and winter) observed and modeled surface concentrations. Using this diagnostic, we find that the modeled sulfate cannot capture the lowest observed values and instead peaks at higher values and has a broader distribution; in addition, the annual mean seems to exhibit a longer tail in the distribution than the observations. Furthermore, the distribution function for elemental carbon is quite well reproduced, except for a higher tendency for small values. On the other hand it is clear that the model simulations of organic carbon cannot capture the mid-range values, especially in the summertime, most likely a representation of the lack of significant SOA production with the current scheme (Lack et al., 2004).

8 Discussion and conclusions

Using a variety of diagnostics and evaluation datasets (including satellite, aircraft, surface measurements and surface data), we have demonstrated the capability of CAM-chem in reasonably representing tropospheric and stratospheric chemistry. In particular, we have shown that the model performs equally well whether forced by analyzed meteorological datasets or by a free-running climate model (in this case forced by observed sea-surface temperature and sea-ice distributions). In addition, owing to the use of a preprocessor, we have shown the capability of this framework to handle separate chemical mechanisms, in addition to previously discussed configurations (e.g.,

GMDD
4, 2199–2278, 2011

Lamarque et al., 2008). Based on the simulations discussed here, we have found that the CO and CH_4 lifetimes are in good agreement with previously published estimates; similarly, our OH distribution is in reasonable agreement with the Spivakovsky et al. (2000) climatology. However, our CO distribution in the high Northern latitudes is underestimated when compared to surface, aircraft and satellite observations, indicating an overestimate of the CO loss by OH or underestimate of its emissions or chemical production. Ozone in the troposphere is simulated reasonably well, with some overestimation of ozone in the upper troposphere/lower stratosphere region in high northern latitudes in comparison to ozone sondes. Even though the model top is limited to 40 km, stratospheric processes are well described. The ozone hole is reasonably well reproduced. Finally, similar to other tropospheric chemistry models (Lin et al., 2008), CAM-chem suffers from a significant overestimate of summertime surface ozone (and other chemical species such as hydrogen peroxide) over the Northeast United States. All necessary inputs (model code and datasets) to perform the simulations described here on a wide variety of computing platforms and compilers can be found at http://www.cesm.ucar.edu/models/cesm1.0/.

Supplementary material related to this article is available online at:
http://www.geosci-model-dev-discuss.net/4/2199/2011/gmdd-4-2199-2011-supplement.pdf.

Acknowledgements. P. G. H. was partially funded under the NSF award 0840825. C. L. H. was partially supported by NSF award 0929282. D. K., J.-F. L. and F. V. were partially funded by the Department of Energy under the SciDAC program. We also acknowledge the science teams producing the data used for model evaluation, including the NOAA Earth System Research Laboratory Global Monitoring Division for surface CO and ozone sondes, and the World Ozone and Ultraviolet Radiation Data Centre (WOUDC) for ozonesondes. The CESM project is supported by the National Science Foundation and the Office of Science (BER) of the US Department of Energy. The National Center for Atmospheric Research is operated by the University Corporation for Atmospheric Research under sponsorship of the National Science Foundation.

GMDD
4, 2199–2278, 2011

References

Aghedo, A. M., Bowman, K. W., Worden, H. M., Kulawik, S. S., Shindell, D. T., Lamarque, J.-F., Faluvegi, G., Parrington, M., Jones, D. B. A., and Rast, S.: The vertical distribution of ozone instantaneous radiative forcing from satellite and chemistry climate models, J. Geophys. Res., 116, D01305, doi:10.1029/2010JD014243, 2011.

Andres, R. and Kasgnoc, A.: A time-averaged inventory of subaerial volcanic sulfur emissions, J. Geophys. Res., 103, 25251–25261, 1998.

Anenberg, S. C., West, J. J., Fiore, A. M., Jaffe, D. A., Prather, M. J., Bergmann, D., Cuvelier, K., Dentener, F. J., Duncan, B. N., Gauss, M., Hess, P., Jonson, J.E., A. Lupu, I.A. MacKenzie, E. Marmer, R. J. Park, M.G. Sanderson, M. Schultz, D.T. Shindell, Szopa, S., Vivanco, M.G., Wild, O., and Zang G.: Intercontinental impacts of ozone pollution on human mortality, Environ. Sci. Technol., 43, 6482–6487, 2009.

Austin, J., Struthers, H., Scinocca, J., Plummer, D., Akiyoshi, H., Baumgaertner, A. J. G., Bekki, S., Bodeker, G. E., Braesicke,P., Bruhl, C., Butchart, N., Chipperfield, M., Cugnet, D., Dameris, M., Dhomse, S., Frith, S., Garny, H., Gettelman, A., Hardiman, S., Jockel, P., Kinnison, D., Lamarque, J.-F., Marchand, M., Michou, M., Morgenstern, O., Nakamura, T., Nielsen, J.E., Pitari, G., Pyle, J., Shepherd, T.G., Shibata, K., Smale, D., Stolarski, R., Teyssedre, H., and Yamashita, Y.: Chemistry climate model simulations of the Antarctic ozone hole, J. Geophys. Res., 115, D00M11, doi:10.1029/2009JD013577, 2010.

Bernath, P. F., McElroy, C. T., Abrams, M. C., Boone, C. D., Butler, M., Camy-Peyret, C., Carleer, M., Clerbaux, C., Coheur, P. F., Colin, R., DeCola, P., DeMaziere, M., Drummond, J., Dufour, D., Evans, W. F. J., Fast, H., Fussen, D., Gilbert, K., Jennings, D. E., Llewellyn, E. J., Lowe, R. P., Mahieu, E., McConnell, J. C., McHugh, M., McLeod, S. D., Michaud, R., Midwinter, C., Nassar, R., Nichitiu, F., Nowlan, C., Rinsland, C. P., Rochon, Y. J., Rowlands, N., Semeniuk, K., Simon, P., Skelton, R., Sloan, J.J., Soucy, M.A., Strong, K., Tremblay, P., Turnbull, D., Walker, K. A., Walkty, I., Wardle, D. A., Wehrle, V., Zander, R. and Zou, J.: Atmospheric Chemistry Experiment (ACE): Mission overview, Geophys. Res. Lett., 32, L15S01, doi:10.1029/2005GL022386, 2005.

Bond, T., Streets, D. G., Yarber, K. F., Nelson, S. M., Woo, J.-H., and Klimont, Z.: A technology-based global inventory of black and organic carbon emissions from combustion, J. Geophys. Res., 109, D14203, doi:10.1029/2003JD003697, 2004.

GMDD
4, 2199–2278, 2011

Boville B. A., Rasch, P. J., Hack, J. J., and McCaa, J. R. : Representation of clouds and precipitation processes in the Community Atmosphere Model version 3 (CAM3), J. Climate, 19, 11, 2184–2198, 2006.

Brasseur G. P., Hauglustaine,D. A., Walters, S., Rasch,P. J., Muller, J.-F. , Granier, C., and Tie, X. X.: MOZART, a global chemical transport model for ozone and related chemical tracers 1. Model description, J. Geophys. Res., 103, D21, 28265–28289, 1998.

Butchart, N., Charlton-Perez, A. J., Cionni, I., Hardiman, S. C., Haynes, P. H., Kruger, K., Kushner, P. J., Newman, P. A., Osprey, S. M., Perlwitz, J., Sigmond, M., Wang, L., Akiyoshi, H., Austin, J., Bekki, S., Baumgaertner, A., Braesicke, P., Bruhl, C., Chipperfield, M., Dameris, M., Dhomse, S., Eyring, V., Garcia, R., Garny, H., Jockel, P., Lamarque, J.-F., Marchand, M., Michou, M., Morgenstern, O., Nakamura, T., Pawson, S., Plummer, D., Pyle, J., Rozanov, E., Scinocca, J., Shepherd, T. G., Shibata, K., Smale, D., Teyssedre, H., Tian, W., Waugh, D. and Yamashita, Y.: Multi-model climate and variability of the stratosphere, J. Geophys. Res., 116, D05102, doi:10.1029/2010JD014995, 2011.

Chen, J., Avise, J., Lamb, B., Salath, E., Mass, C., Guenther, A., Wiedinmyer, C., Lamarque, J.-F., O'Neill, S., McKenzie, D., and Larkin, N.: The effects of global changes upon regional ozone pollution in the United States, Atmos. Chem. Phys., 9, 1125–1141, doi:10.5194/acp-9-1125-2009, 2009.

Collins W. D., Rasch, P. J., Boville, B. A., Hack, J. J., McCaa, J. R., Williamson, D. L., Briegleb, B., Bitz, C. M., Lin, S.-J., and Zhang, M.: The Community Climate System Model version 3 (CCSM3), J. Climate, 19, 2122–2143, 2006.

Cooke, W. F., Liousse, C., Cachier, H., and Feichter, J.: Construction of a 1x1 fossil fuel emission data set for carbonaceous aerosol and implementation and radiative impact in the ECHAM4 model, J. Geophys. Res., 104 (D18), 22137–22162, 1999.

Cooper, M., Martin, R. V., Sauvage, B., Boone, C. D., Walker, K. A., Bernath, P. F., McLinden, C. A., Degenstein, D. A., Volz-Thomas, A., and Wespes, C.: Evaluation of ACE-FTS and OSIRIS Satellite retrievals of ozone and nitric acid in the tropical upper troposphere: Application to ozone production efficiency, J. Geophys. Res., 116, D12306, doi:10.1029/2010JD015056, 2011.

DeCaria, A. J., Pickering, K. E., Stenchikov, G. L., and Ott, L. E.: Lightning-generated NOX and its impact on tropospheric ozone production: Athree-dimensional modeling study of a Stratosphere-Troposphere Experiment:Radiation, Aerosols and Ozone (STERAO-A) thunderstorm, J. Geophys. Res., 110, D14303, doi:10.1029/2004JD005556, 2006.

GMDD

4, 2199–2278, 2011

Deeter, M., Edwards, D. P., Gille, J. C., Emmons, L. K., Francis, G., Ho, S.-P., Mao, D., Masters, D., Worden, H., Yudin, V., and Drummond, J. R.: The MOPITT Version 4 CO product: Algorithm enhancements, selected results and bias drift, J. Geophys. Res., 115, D07306, doi:10.1029/2009JD013005, 2010.

Emmons, L. K., Hauglustaine, D. A., Müller, J.-F., Carroll, M. A., Brasseur, G. P., Brunner, D., Staehelin, J., Thouret, V., and Marenco, A.: Data composites of airborne observations of tropospheric ozone and its precursors, J. Geophys. Res., 105, 20497–20538, 2000.

Emmons, L. K., Walters, S., Hess, P. G., Lamarque, J.-F., Pfister, G. G., Fillmore, D., Granier, C., Guenther, A., Kinnison, D., Laepple, T., Orlando, J., Tie, X., Tyndall, G., Wiedinmyer, C., Baughcum, S. L., and Kloster, S.: Description and evaluation of the Model for Ozone and Related chemical Tracers, version 4 (MOZART-4), Geosci. Model Dev., 3, 43–67, doi:10.5194/gmd-3-43-2010, 2010.

Fiore, A. M., Dentener, F. J., Wild, O., Cuvelier, C., Schultz, M. G., Hess, P., Textor, C., Schulz, M., Doherty, R. M., Horowitz, I. A., MacKenzie, M. G., Sanderson, D. T. Shindell, D. S., Stevenson, S., Szopa, R., Van Dingenen, G., Zeng, C., Atherton, D., Berg, L. W. mann, I. Bey, G., Carmichael, W. J., Collins, B. N., Duncan, G., Faluvegi, G., Folberth, M., Gauss, S., Gong, D., Hauglustaine, T., Holloway, I. S. A., Isaksen, D. J., Jacob, J. E., Jonson, J. W., Kaminski, T. J., Keating, A., Lupu, E., Marmer, V., Montanaro, R. J., Park, G., Pitari, K. J., Pringle, J. A., Pyle, S., Schroeder, M. G., Vivanco, P., Wind, G., Wojcik, S., Wu, and Zuber, A.: Multi-Model estimates of intercontinental source-receptor relationships for ozone pollution, J. Geophys. Res., D04301, doi:10.1029/2008JD010816, 2009.

Forster, P. V., Ramaswamy, V., Artaxo, P., Berntsen, T., Betts, R., Fahey, D. W., Haywood, J., Lean, J., Lowe, D. C., Myhre, G., Nganga, J., Prinn, R., Raga, G., Schulz, M., and Van Dorland, R.: Changes in Atmospheric Constituents and in Radiative Forcing. In: Climate Change 2007: The Physical Science Basis, Contribution of Working Group I to the Fourth Assessment Report of the Intergovernmental Panel on Climate Change, edited by: Solomon, S., Qin, D., Manning, M., Chen, Z., Marquis, M., Averyt, K. B., Tignor, M., and Miller, H. L., Cambridge University Press, Cambridge, UK and New York, NY, USA, 2007.

Garcia, R. R., Marsh, D. R., Kinnison, D. E., Boville, B. A., and Sassi, F.: Simulation of secular trends in the middle atmosphere, 1950–2003, J. Geophys. Res., 112, doi:10.1029/2006JD007485, 2007.

Granier, C., Guenther, A., Lamarque, J., Mieville, A., Muller, J., Olivier, J., Orlando, J., Peters, J., Petron, G., Tyndall, G., and Wallens, S.: POET, a database of surface emissions ofozone

GMDD
4, 2199–2278, 2011

precursors, available at: http://www.aero.jussieu.fr/projet/ACCENT/POET.php, (last access: August 2008), 2005.
Grooß, J.-U. and Russell III, J. M.: Technical note: A stratospheric climatology for O_3, H_2O, CH_4, NO_x, HCl and HF derived from HALOE measurements, Atmos. Chem. Phys., 5, 2797–2807, doi:10.5194/acp-5-2797-2005, 2005.
Guenther, A., Hewitt, C. N., Erickson, D., Fall, R., Geron, C., Graedel, T., Harley, P., Klinger, L., Lerdau, M., McKay, W., Pierce, T., Scholes, B., Steinbrecher, R., Tallamraju, R., Taylor, J., and Zimmerman, P.: A global model of natural volatile organic compound emissions, J. Geophys. Res., 100, 8873–8892, 1995.
Guenther, A., Karl, T., Harley, P., Wiedinmyer, C., Palmer, P. I., and Geron, C.: Estimates of global terrestrial isoprene emissions using MEGAN (Model of Emissions of Gases and Aerosols from Nature), Atmos. Chem. Phys., 6, 3181–3210, doi:10.5194/acp-6-3181-2006, 2006.
Hack, J. J., Caron, J. M., Yeager, S. G., Oleson, K. W., Holland, M. M., Truesdale, J. E., and Rasch, P. J.: Simulation of the global hydrological cycle in the CCSM Community Atmosphere Model Version 3 (CAM3): Mean features, J. Climate, 2199–2221, 2006.
Heald, C. L., Henze, D. K., Horowitz, L. W., Feddema, J., Lamarque, J.-F., Guenther, A., Hess, P. G., Vitt, F., Seinfeld, J. H., Goldstein, A. H., and Fung, I.: Predicted change in global secondary organic aerosol concentrations in response to future climate, emissions, and land-use change, J. Geophys. Res., 113, D05211, doi:10.1029/2007JD009092, 2008.
Holtslag, A. A. M. and Boville, B. A.: Local versus nonlocal boundary layer diffusion in a global climate model, J. Climate, 6, 1825–1841, 1993.
Horowitz, L. W., Walters, S., Mauzerall, D. L., Emmons, L. K., Rasch, P. J., Granier, C., Tie, X. X., Lamarque, J.-F., Schultz, M. G., Tyndall, G. S., Orlando, J. J., and Brasseur, G. P.: A global simulation of tropospheric ozone and related tracers: Description and evaluation of MOZART, version 2, J. Geophys. Res., 108(D24), 4784, doi:10.1029/2002JD002853, 2003.
Hsu, J., Prather, M. J., and Wild, O.: Diagnosing the stratosphere-to-troposphere flux of ozone in a chemistry transport model, J. Geophys. Res., 110, D19305, doi:10.1029/2005JD006045, 2005.
Jacob, D. J. and Winner, D. A.: Effect of Climate Change on Air Quality, Atmos. Environ. 43(1), 392, 51–63, doi:10.1016/j.atmosenv.2008.09.05, 2009.
Jakob, C. and Klein, S. A.: A parametrization of cloud and precipitation overlap effects for use in General Circulation Models, Q. J. Roy. Meteorol. Soc., 126, 2525–2544, 2000.

GMDD
4, 2199–2278, 2011

Jonson, J. E., Stohl, A., Fiore, A. M., Hess, P., Szopa, S., Wild, O., Zeng, G., Dentener, F. J., Lupu, A., Schultz, M. G., Duncan, B. N., Sudo, K., Wind, P., Schulz, M., Marmer, E., Cuvelier, C., Keating, T., Zuber, A., Valdebenito, A., Dorokhov, V., De Backer, H., Davies, J., Chen, G. H., Johnson, B., Tarasick, D. W., Stübi, R., Newchurch, M. J., von der Gathen, P., Steinbrecht, W., and Claude, H.: A multi-model analysis of vertical ozone profiles, Atmos. Chem. Phys., 10, 5759–5783, doi:10.5194/acp-10-5759-2010, 2010.

Kärcher, B. and Voigt, C.: Formation of nitric acid/water ice particles in cirrus clouds, Geophys. Res. Lett., 33, L08806, doi:10.1029/2006GL025927, 2006.

Kinnison, D. E., Brasseur, G. P., Walters, S., Garcia, R. R., Marsh, D. A., Sassi, F., Boville, B. A., Harvey, L., Randall, C., Emmons, L., Lamarque, J.-F., Hess, P., Orlando, J., Tyndall, G., Tie, X. X., Randel, W., Pan, L., Gettelman, A., Granier, C., Diehl, T., Niemeier, U. and Simmons, A. J.: Sensitivity of chemical tracers to meteorological parameters in the MOZART-3 chemical transport model, J. Geophys. Res., 112, D20302, doi:10.1029/2006JD007879, 2007.

Kinnison, D. E. Marsh, D. R., Garcia, R. R., Vitt, F., Tilmes, S., Mills, M. J., Lamarque, J.-F., Emmons, L. K., Orlando, J. J., Gettelman, A., Liu, H.-L., Yudin, V., Park, M., Randel, W., Pan, L. L., Brakebusch, M., Randall, C. E., and Hess, P.: Description and evaluation of the Whole Atmosphere Community Climate Model (WACCM): Chemistry Update, in preparation, 2011.

Kloster, S., Feichter, J., Maier-Reimer, E., Six, K. D., Stier, P., and Wetzel, P.: DMS cycle in the marine ocean-atmosphere system – a global model study, Biogeosciences, 3, 29–51, doi:10.5194/bg-3-29-2006, 2006.

Lack, D. A., Tie, X. X., Bofinger, N. D., Wiegand, A. N., and Madronich, S.: Seasonal variability of secondary organic aerosol: A global modeling study, J. Geophys. Res., 109, D03202, doi:10.1029/2003JD003418, 2004.

Lamarque, J.-F. and Solomon, S.: Impact of Changes in Climate and Halocarbons on Recent Lower Stratosphere Ozone and Temperature Trends, J. Climate, 23, 2599–2611, 2010.

Lamarque, J.-F., Kiehl, J. T., Hess, P. G., Collins, W. D., Emmons, L. K., Ginoux, P., Luo, C., and Tie, X. X.: Response of a coupled chemistry-climate model to changes in aerosol emissions: Global impact on the hydrological cycle and the tropospheric burdens of OH, ozone and NOx. Geophys. Res. Lett., 32, 16, L16809, doi:10.1029/2005GL023419, 2005.

Lamarque, J.-F., Kinnison, D. E., Hess, P. G., and Vitt, F.: Simulated lower stratospheric trends between 1970 and 2005: identifying the role of climate and composition changes, J. Geophys. Res., 113, D12301, doi:10.1029/2007JD009277, 2008.

GMDD
4, 2199–2278, 2011

Lamarque, J.-F., Bond, T. C., Eyring, V., Granier, C., Heil, A., Klimont, Z., Lee, D., Liousse, C., Mieville, A., Owen, B., Schultz, M. G., Shindell, D., Smith, S. J., Stehfest, E., Van Aardenne, J., Cooper, O. R., Kainuma, M., Mahowald, N., McConnell, J. R., Naik, V., Riahi, K., and van Vuuren, D. P.: Historical (1850–2000) gridded anthropogenic and biomass burning emissions of reactive gases and aerosols: methodology and application, Atmos. Chem. Phys., 10, 7017–7039, doi:10.5194/acp-10-7017-2010, 2010.

Lamarque, J.-F., McConnell, J. R., Shindell, D. T., Orlando, J. J., and Tyndall, G. S.: Understanding the drivers for the 20th century change of hydrogen peroxide in Antarctic ice-cores. Geophys. Res. Lett., 38, L04810, doi:10.1029/2010GL045992, 2011a.

Lamarque, J.-F., Kyle, G. P., Meinshausen, M., Riahi, K., Smith, S. J., van Vuuren, D. P., Conley, A., and Vitt, F.: Global and regional evolution of short-lived radiatively-active gases and aerosols in the Representative Concentration Pathways, Climatic Change, Online First, 5 August 2011, 2011b.

Lauritzen, P. H., Ullrich, P. A., and Nair, R. D.: Atmospheric transport schemes: Desirable properties and a semi-Lagrangian view on finite-volume discretizations, in Numerical Techniques for Global Atmospheric Models, Lect. Notes Comp. Sci., 80, Springer, Berlin, 2011.

Lawrence, M. G., Jockel, P., and von Kuhlmann, R.: What does the global mean OH concentration tell us?, Atmos. Chem. Phys., 1, 37–49, doi:10.5194/acp-1-37-2001, 2001.

Lawrence, P. J. and Chase, T. N.: Representing a new MODIS consistent land surface in the Community Land Model (CLM 3.0), J. Geophys. Res., 112, G01023, doi:10.1029/2006JG000168, 2007.

Levis, S., Wiedinmyer, C., Guenther, A., and Bonan, G.: Coupling Biogenic VOC Emissions to the Community Land Model: Effects of Land Use Change on BVOC emissions, J. Geophys. Res. , 108, D21, 4659, doi:10.1029/2002JD003203, 2003.

Liao, H., Adams, P. J., Chung, S. H., Seinfeld, J. H., Mickley, L. J., and Jacob, D. J.: Interactions between tropospheric chemistry and aerosols in a unified general circulation model, J. Geophys. Res. 108, 4001, doi:10.1029/2001JD001260, 2003.

Lin, J.-T., Youn, D., Liang, X.-Z., and Wuebbles, D. J.: Global model simulation of summertime US ozone diurnal cycle and its sensitivity to PBL mixing, spatial resolution, and emissions, Atmos. Environ., doi:10.1016/j.atmosenv.2008.08.012, 2008.

Logan, J. A.: Trends in the vertical distribution of ozone: An analysis of ozonesonde data, J. Geophys. Res., 99, 25553–25585, 1994.

GMDD
4, 2199–2278, 2011

Lowe, D. and Mackenzie, R.: Review of polar stratospheric cloud microphysics and chemistry, J. Atmos Solar-Terr. Phys., 70, 13–40, 2008.
Madronich, S.: Photodissociation in the atmosphere 1. Actinic flux and the effects of ground reflections and clouds, J. Geophys. Res., 92, 9740–9752, 1987.
Mahowald, N., Lamarque, J.-F., Tie, X. X., and Wolff, E: Sea-salt aerosol response to climate change: Last Glacial Maximum, preindustrial, and doubled carbon dioxide climates, J. Geophys. Res., 111, D05303, doi:10.1029/2005JD006459, 2006a.
Mahowald, N. M., Muhs, D. R., Levis, S., Rasch, P. J., Yoshioka, M., Zender, C. S., and Luo, C.: Change in atmospheric mineral aerosols in response to climate: Last glacial period, preindustrial, modern, and doubled carbon dioxide climates, J. Geophys. Res., 111, D10202, 10210.11029/12005JD006653, 2006b.
Malm, W. C., Schichtel, B. A., Pitchford, M. L., Ashbaugh L. L., and Eldred, R. A.: Spatial and monthly trends in speciated fine particle concentration in the United States, J. Geophys. Res., 109, doi:10.1029/2003JD003739, 2004.
McLinden, C., Olsen, S., Hannegan, B., Wild, O., and Prather, M.: Stratospheric ozone in 3-D models: A simple chemistry and the cross-tropopause flux, J. Geophys. Res., 105, 14653–14665, 2000.
Meinshausen, M., Smith, S. J., Calvin, K., Daniel, J. S., Kainuma, M. L. T., Lamarque, J.-F., Matsumoto, K., Montzka, S., Raper, S., Riahi, K., Thomson, A., Velders, G. J. M., and van Vuuren, D. P.: The RCP Greenhouse Gas Concentrations and their Extensions from 1765 to 2300, Climatic Change, Online First, 5 August 2011, 2011.
Metzger, S., Dentener, F., Pandis, S., and Lelieveld, J.: Gas/aerosol partitioning: 1. A computationally efficient model, J. Geophys. Res., 107(D16), 4312, doi:10.1029/2001JD001102, 2002.
Morgenstern, O., Akiyoshi, H.H., Bekki, S., Braesicke, P., Chipperfield, M., Gettelman, A., Hardiman, S., Lamarque, J.-F., Michou, M., Pawson, S., Rozanov, E., Scinocca, J., Shibata, K., and Smale, D.: Anthropogenic forcing of the Northern Annular Mode in CCMVal-2 models, J. Geophys. Res., 115, D00M03, doi:10.1029/2009JD013347, 2010.
Neale, R. B., Richter, J., Park, S., Lauritzen, P. H., Vavrus, S. J., Rasch, P. J., and Zhang, M.: The Mean Climate of the Community Atmosphere Model (CAM4) in Forced SST and Fully Coupled Experiments, J. Climate, submitted, 2011.
Neu, J. L. and Prather, M. J.: Toward a more physical representation of precipitation scavenging in global chemistry models: cloud overlap and ice physics and their impact on tropospheric

GMDD
4, 2199–2278, 2011

ozone, Atmos. Chem. Phys. Discuss., 11, 24413–24466, doi:10.5194/acpd-11-24413-2011, 2011.
Novelli, P. C., Masarie, K. A., Lang, P. M., Hall, B. D., Myers R. C., and Elkins, J. W.: Reanalysis of tropospheric CO trends: Effects of the 1997–1998 wildfires, J. Geophys. Res., 108, doi:101029/2002JD003031, 2003.
Ohara, T., Akimoto, H., Kurokawa, J., Horii, N., Yamaji, K., Yan, X., and Hayasaka, T.: An Asian emission inventory of anthropogenic emission sources for the period 1980–2020, Atmos. Chem. Phys., 7, 4419–4444, doi:10.5194/acp-7-4419-2007, 2007.
Pfister, G., Hess, P. G., Emmons, L. K., Rasch, P. J., and Vitt, F. M.: Impact of the Summer 2004 Alaska Fires on TOA Clear-Sky Radiation Fluxes, J. Geophys. Res., 113, D02204, doi:10.1029/2007JD008797, 2008.
Prather, M. J.: Tropospheric O_3 from photolysis of O_2, Geophys. Res. Lett., 36, L03811, doi:10.1029/2008GL036851, 2009.
Price, C. and Rind, D.: A simple lightning parameterization for calculating global lightning distributions, J. Geophys. Res., 97, 9919–9933, doi:10.1029/92JD00719, 1992.
Price, C., Penner, J., and Prather, M.: NO_x from lightning 1. Global distribution based on lightning physics, J. Geophys. Res., 102, 5929–5941, 1997.
Randerson, J., Liu, H., Flanner, M. G., Chambers, S. D., Jin, Y., Hess, P. G., Pfister, G., Mack, M. C., Treseder, K. K., Welp, L. R., Chapin, F. S., Harden, J. W., Goulden, M. L., Lyons, E., Neff, J. C., Schuur E. A. G., and Zender, C. S.: The Impact of Boreal Forest Fires on Climate Warming, Science, 314, 1130–1132, doi:10.1126/science.1132075, 2006.
Rasch, P. J., Mahowald, N. M., and Eaton, B. E.: Representations of transport, convection, and the hydrologic cycle in chemical transport models: Implications for the modeling of short-lived and soluble species, J. Geophys. Res., 102, D23, 28127–28138, 1997.
Rasch P. J., Coleman, D. B., Mahowald, N., WIlliamson, D. L., Lin, S.-J., Boville, B. A., and Hess, P.: Characteristics of atmospheric transport using three numerical formulations for atmospheric dynamics in a single GCM framework, J. Climate, 19, 11, 2243–2266, 2006.
Ridley, B., Pickering, K., and Dye, J. : Comments on the parameterization of lightning-produced NO in global chemistry-transport models, Atmos. Environ., 39, 6184–6187, 2005.
Rotman, D., Atherton, C. S., Bergmann, D. J., Cameron-Smith, P. J., Chuang, C. C., Connell, P. S., Dignon, J. E., Franz, A., Grant, K. E., Kinnison, D. E., Molenkamp, C. R., Proctor, D. D., and Tannahill, J. R.: IMPACT, the LLNL 3-D global atmospheric chemical transport model for the combined troposphere and stratosphere: Model description and analysis of ozone and

GMDD
4, 2199–2278, 2011

other trace gases, J. Geophys. Res., 109, D04303, doi:10.1029/2002JD003155, 2004.
Rotstayn, L. D. and Lohmann, U. : Tropical rainfall trends and the indirect aerosol effect, J. Climate, 15, 2103–2116, 2002.
Sander, S. P., Friedl, R. R., Golden, D. M., Kurylo, M J., Moortgat, G. K., Wine, P. H., Ravishankara, A. R., Kolb, C. E., Molina, M. J., Finlayson-Pitts, B. J., Huie, R. E., and Orkin, V.: Chemical Kinetics and Photochemical Data for Use in Atmospheric Studies – Evaluation Number 15, JPL Publication 06-2, 2006.
Sanderson, M., Collins, W., Derwent, R., and Johnson, C.: Simulation of global hydrogen levels using a Lagrangian three-dimensional model, J. Atmos. Chem., 46, 15–28, 2003.
Sanderson, M. G. Dentener, F. J., Fiore, A. M., Cuvelier, C., Keating, T. J., Zuber, A., Atherton, C. S., Bergmann, D. J., Diehl, T., Doherty, R. M., Duncan, B. N., Hess, P., Horowitz, L. W., Jacob, D. J., Jonson, J.-E., Kaminski, J. W., Lupu, A., MacKenzie, I. A., Mancini, E., Marmer, E., Park, R., Pitari, G., Prather, M. J., Pringle, K. J., Schroeder, S., Schultz, M. G., Shindell, D. T., Szopa, S., Wild, O., and Wind, P.: A multi-model source-receptor study of the hemispheric transport and deposition of oxidised nitrogen. Geophys. Res. Lett., 35, L17815, doi:10.1029/2008GL035389, 2008.
Shindell, D. T., Faluvegi, G., Stevenson, D. S., Krol, M. C., Emmons, L. K., Lamarque, J. F., Petron, G., Dentener, F. J., Ellingson, K., Schultz, M. G., Wild, O., Amann, M., Atherton, C. S., Bergmann, D. J., Bey, I., Butler, T., Cofala, J., Collins, W. J., Derwent, R. G., Doherty, R. M., Drevet, J., Eskes, H. J., Fiore, A. M., Gauss, M., Hauglustaine, D. A., Horowitz, L. W., Isaksen, I. S. A., Lawrence, M. G., Montanaro, V., Muller, J. F., Pitari, G., Prather, M. J., Pyle, J. A., Rast, S., Rodriguez, J. M., Sanderson, M. G., Savage, N. H., Strahan, S. E., Sudo, K., Szopa, S., Unger, N., van Noije, T. P. C, and Zen, G.: Multi-model simulations of carbon monoxide: Comparison with observations and projected near-future changes, J. Geophys. Res., 111, D19306, doi:10.1029/2006JD007100, 2006.
Shindell, D. T., Chin, M., Dentener, F., Doherty, R. M., Faluvegi, G., Fiore, A. M., Hess, P., Koch, D. M., MacKenzie, I. A., Sanderson, M. G., Schultz, M. G., Schulz, M., Stevenson, D. S., Teich, H., Textor, C., Wild, O., Bergmann, D. J., Bey, I., Bian, H., Cuvelier, C., Duncan, B. N., Folberth, G., Horowitz, L. W., Jonson, J., Kaminski, J. W., Marmer, E., Park, R., Pringle, K. J., Schroeder, S., Szopa, S., Takemura, T., Zeng, G., Keating, T. J., and Zuber, A.: A multi-model assessment of pollution transport to the Arctic, Atmos. Chem. Phys., 8, 5353–5372, doi:10.5194/acp-8-5353-2008, 2008.

GMDD
4, 2199–2278, 2011

Singh, H. B., Brune, W. H., Crawford, J. H., Jacob, D. J., and Russell, P. B.: Overview of the summer 2004 Intercontinental Chemical Transport Experiment-North America (INTEX-A), J. Geophys. Res., 111, D24S01, doi:10.1029/2006JD007905, 2006.

Singh, H. B., Brune, W. H., Crawford, J. H., Flocke, F., and Jacob, D. J.: Chemistry and transport of pollution over the Gulf of Mexico and the Pacific: spring 2006 INTEX-B campaign overview and first results, Atmos. Chem. Phys., 9, 2301–2318, doi:10.5194/acp-9-2301-2009, 2009.

SPARC CCMVal: Report on the Evaluation of Chemistry-Climate Models, edited by: Eyring, V., Shepherd, T. G., Waugh, D. W., SPARC Repot No.4, WCRP-X, WMO/TD-No. X, http://www.atmosp.physics.utoronto.ca/SPARC, 2010.

Sparks, J. P., Roberts, J. M., and Monson, R. K.: The uptake of gaseous organic nitrogen by leaves: A significant global nitrogen transfer process, Geophys. Res. Lett., 30, 2189, doi:10.1029/2003GL018578, 2003.

Spivakovsky, C. M., Logan, J. A., Montzka, S. A., Balkanski, Y. J., Foreman-Fowler, M., Jones, D. B. A., Horowitz, L. W., Fusco, A. C., Brenninkmeijer, C. A. M., Prather, M. J., Wofsy, S. C., and McElroy, M. B.: Three-dimensional climatological distribution of tropospheric OH: Update and evaluation, J. Geophys. Res., 105, 8931–8980, 2000.

Stevenson, D. S., Dentener, F. J., Schultz, M. G., Ellingsen, K., van Noije, T. P. C., Wild, O., Zeng, G., Amann, M., Atherton, C. S., Bell, N., Bergmann, D. J., Bey, I., Butler, T., Cofala, J., Collins, W. J., Derwent, R. G., Doherty, R. M., Drevet, J., Eskes, H. J., Fiore, A. M., Gauss, M., Hauglustaine, D. A., Horowitz, L. W., Isaksen, I. S. A., Krol, M. C., Lamarque, J.-F., Lawrence, M. G., Montanaro, V., Muller, J.-F., Pitari, G., Prather, M. J., Pyle, J. A., Rast, S., Rodriguez, J. M., Sanderson, M. G., Savage, N. H., Shindell, D. T., Strahan, S. E., Sudo, K., and Szopa, S.: Multi-model ensemble simulations of present-day andnear-future tropospheric ozone, J. Geophys. Res., 111, D08301, doi:10.1029/2005JD006338, 2005.

Tie, X., Brasseur, G., Emmons, L., Horowitz, L., and Kinnison, D.: Effects of aerosols on tropospheric oxidants: A global model study, J. Geophys. Res., 106, 22931–22964, 2001.

Tie, X., Madronich, S., Walters, S., Edwards, D. P., Ginoux, P., Mahowald, N., Zhang, R., Lou, C., and Brasseur, G.: Assessment of the global impact of aerosols on tropospheric oxidants, J. Geophys. Res., 110, D03204, doi:10.1029/2004JD005359, 2005.

Turnipseed, A., Huey, G., Nemitz, E., Stickel, R., Higgs, J., Tanner, D., Slusher, D., Sparks, J., Flocke, F., and Guenther, A.: Eddy covariance fluxes of peroxyacyl nitrates (PANs) and NOy to a coniferous forest, J. Geophys. Res., 111, D09304, doi:10.1029/2005JD006631, 2006.

van der Werf, G. R., Randerson, J. T., Giglio, L., Collatz, G. J., Kasibhatla, P. S., and Arellano

GMDD
4, 2199–2278, 2011

Jr., A. F.: Interannual variability in global biomass burning emissions from 1997 to 2004, Atmos. Chem. Phys., 6, 3423–3441, doi:10.5194/acp-6-3423-2006, 2006.
Walcek, C. J., Brost, R. A., Chang, J. S., and Wesely, M. L.: SO_2, sulfate and HNO_3 deposition velocities computed using regional landuse and meteorological data, Atmos. Environ., 20, 946–964, 1986.
Walmsley, J. L. and Wesely, M. L.: Modification of coded parameterizations of surface resistances to gaseous dry deposition, Atmos. Environ., 30, 1181–1188, 1996.
Wesely, M. L.: Parameterizations for surface resistance to gaseous dry deposition in regional-scale numerical models, Atmos. Environ., 23, 1293–1304, 1989.
Wesely, M. L. and Hicks, B. B.: A review of the current status of knowledge on dry deposition, Atmos. Environ., 34, 2261–2282, 2000.
Wiedinmyer, C., Akagi, S. K., Yokelson, R. J., Emmons, L. K., Al-Saadi, J. A., Orlando, J. J., and Soja, A. J.: The Fire INventory from NCAR (FINN) – a high resolution global model to estimate the emissions from open burning, Geosci. Model Dev. Discuss., 3, 2439–2476, doi:10.5194/gmdd-3-2439-2010, 2010.
Wild, O. and Prather, M. J.: Global tropospheric ozone modelling: Quantifying errors due to grid resolution, J. Geophys. Res., 111(D11), D11305, doi:10.1029/2005JD006605, 2006.
Yonemura, S., Kawashima, S., and Tsuruta, H.: Carbon monoxide, hydrogen, and methane uptake by soils in a temperate arable field and a forest, J. Geophys. Res., 105, 14347–14362, 2000.
Zhang, G. J. and McFarlane, N. A.: Sensitivity of climate simulations to the parameterization of cumulus convection in the Canadian Climate Centre general circulation model, Atmos. Ocean., 33, 407–446, 1995.

GMDD
4, 2199–2278, 2011

Table 1. Plant functional types in land model of the CESM.

Index	Plant functional type
1	desert, ice and ocean
2	needleleaf evergreen temperate tree
3	needleleaf evergreen boreal tree
4	needleleaf deciduous temperate tree
5	broadleaf evergreen tropical tree
6	broadleaf evergreen temperate tree
7	broadleaf deciduous tropical tree
8	broadleaf deciduous temperate tree
9	broadleaf deciduous boreal tree
10	broadleaf evergreen shrub
11	broadleaf deciduous temperate shrub
12	broadleaf deciduous boreal shrub
13	C_3 arctic grass
14	C_3 non-arctic grass
15	C_4 grass
16	corn
17	wheat

GMDD
4, 2199–2278, 2011

Table 2. List of input fields required for specified dynamics in CAM.

Variable	Physical description (units, geometric dimensions)
U	zonal wind component ($m\,s^{-1}$, 3-D)
V	meridional wind component ($m\,s^{-1}$, 3-D)
T	temperature (K, 3-D)
PS	surface pressure (Pa, 2-D)
PHIS	surface geopotential ($m^2\,s^{-2}$, 2-D)
TS	surface temperature (K, 2-D)
TAUX	zonal surface stress ($N\,m^{-2}$, 2-D)
TAUY	meridional surface stress ($N\,m^{-2}$, 2-D)
SHFLX	sensible heat flux ($W\,m^{-2}$, 2-D)
LHFLX	latent heat flux ($W\,m^{-2}$, 2-D), computed from moisture flux
OCNFRAC	Grid cell fraction over ocean used in dry deposition (2-D)
ICEFRAC	Grid cell fraction over ocean ice used in dry deposition, based on meteorology surface temperatures (2-D)

GMDD
4, 2199–2278, 2011

Table 3. List of species in the considered chemical mechanisms. In addition, we list the chemical solver (Explicit or Implicit), the potential use of emissions of lower-boundary conditions and of deposition processes (wet and dry).

Number	Species name*	Formula	Solver	Emissions	Boundary condition	Wet deposition	Dry deposition
1	ALKO2	$C_5H_{11}O_2$	I				
2	ALKOOH	$C_5H_{12}O_2$	I			X	X
3	BIGALD	$C_5H_6O_2$	I	X			
4	BIGALK	C_5H_{12}	I	X			
5	BIGENE	C_4H_8	I	X			
6	C10H16		I	X			
7	C2H2		I	X			
8	C2H4		I	X			
9	C2H5O2		I				
0	C2H5OH		I	X		X	X
11	C2H5OOH		I			X	X
12	C2H6		I	X			
13	C3H6		I	X			
14	C3H7O2		I				
15	C3H7OOH		I			X	
16	C3H8		I	X			
17	CH2O		I	X		X	X
18	CH3CHO		I	X		X	X
19	CH3CN		I	X		X	X
20	CH3CO3		I				
21	CH3COCH3		I	X			X
22	CH3COCHO		I				X
23	CH3COOH		I	X		X	X
24	CH3COOOH		I			X	X
25	CH3O2		I				
26	CH3OH		I	X		X	X
27	CH3OOH		I			X	
28	CH4		E		X		
29	CO		E	X			X
30	CRESOL	C_7H_8O	I				
31	DMS	CH_3SCH_3	I	X			
32	ENEO2	$C_4H_9O_3$	I				
33	EO	$HOCH_2CH_2O$	I				
34	EO2	$HOCH_2CH_2O_2$	I				
35	GLYALD	$HOCH_2CHO$	I			X	X
36	GLYOXAL	$C_2H_2O_2$	I				
37	H2		E		X		
38	H2O2		I			X	X
39	HCN		I	X		X	X
40	HCOOH		I	X		X	X

* The convention in the "Species name" column refers to the actual naming as it appears in the code (limited to 8 characters). All chemistry subroutines can identify the array index for a specific species through query functions associated with the name as listed here.

GMDD
4, 2199–2278, 2011

Table 3. Continued.

Number	Species name	Formula	Solver	Emissions	Boundary condition	Wet deposition	Dry deposition
41	HNO3		I			X	X
42	HO2		I				
43	HOCH2OO		I				
44	HO2NO2		I			X	X
45	HYAC	CH_3COCH_2OH	I			X	X
46	HYDRALD	$HOCH_2CCH_3CHCHO$	I			X	X
47	ISOP	C_5H_8	I	X			
48	ISOPNO3	$CH_2CHCCH_3OOCH_2ONO_2$	I			X	
49	ISOPO2	$HOCH_2COOCH_3CHCH_2$	I				
50	ISOPOOH	$HOCH_2COOHCH_3CHCH_2$	I			X	X
51	MACR	CH_2CCH_3CHO	I			X	
52	MACRO2	$CH_3COCHO_2CH_2OH$	I				
53	MACROOH	$CH_3COCHOOHCH_2OH$	I			X	X
54	MCO3	$CH_2CCH_3CO_3$	I				
55	MEK	C_4H_8O	I	X			
56	MEKO2	$C_4H_7O_3$	I				
57	MEKOOH	$C_4H_8O_3$	I			X	X
58	MPAN	$CH_2CCH_3CO_3NO_2$	I				X
59	MVK	$CH_2CHCOCH_3$	I			X	
60	N2O		E		X		
61	N2O5		I				
62	NH3		I	X		X	X
63	NO		I	X			X
64	NO2		I	X			X
65	NO3		I				
66	O		I				
67	O1D	O	I				
68	O3		I				X
69	OH		I				
70	ONIT	$CH_3COCH_2ONO_2$	I			X	X
71	ONITR	$CH_2CCH_3CHONO_2CH_2OH$	I			X	X
72	Pb		E				X
73	PAN	$CH_3CO_3NO_2$	I				X
74	PO2	$C_3H_6OHO_2$	I				
75	POOH	C_3H_6OHOOH	I			X	X
76	Rn		E	X			
77	RO2	$CH_3COCH_2O_2$	I				
78	ROOH	CH_3COCH_2OOH	I			X	X
79	SO2		I	X		X	X
80	TERPO2	$C_{10}H_{17}O_3$	I				

GMDD
4, 2199–2278, 2011

Table 3. Continued.

Number	Species name	Formula	Solver	Emissions	Boundary condition	Wet deposition	Dry deposition
81	TERPOOH	$C_{10}H18O_3$	I			X	X
82	TOLO2	$C_7H_9O_5$	I				
83	TOLOOH	$C_7H_{10}O_5$	I			X	X
84	TOLUENE	C_7H_8	I	X			
85	XO2	$HOCH_2COOCH_3CHOHCHO$	I				
86	XOH	$C_7H_{10}O_6$	I				
87	XOOH	$HOCH_2COOHCH_3CHOHCHO$	I			X	X
	Bulk aerosol species						
n 1	CB1	C, hydrophobic black carbon	I	X			X
2	CB2	C, hydrophilic black carbon	I	X		X	X
3	DST01	$AlSiO_5$	I	X		X	X
4	DST02	$AlSiO_5$	I	X		X	X
5	DST03	$AlSiO_5$	I	X		X	X
6	DST04	$AlSiO_5$	I	X		X	X
7	NH4		I			X	X
8	NH4NO3		I			X	X
9	OC1	C, hydrophobic organic carbon	I	X			X
10	OC2	C, hydrophilic organic carbon	I	X		X	X
11	SOA	C_{12}	I			X	X
12	SO4		I	X		X	X
13	SSLT01	NaCl	I	X		X	X
14	SSLT02	NaCl	I	X		X	X
15	SSLT03	NaCl	I	X		X	X
16	SSLT04	NaCl	I	X		X	X
	Stratospheric species						
n 1	BRCL	BrCl	I				
2	BR	Br	I				
3	BRO	BrO	I				
4	BRONO2	$BrONO_2$	I			X	
5	BRY		E		X		
6	CCL4	CCl_4	E		X		
7	CF2CLBR	CF_2ClBr	E		X		
8	CF3BR	CF_3Br	E		X		
9	CFC11	$CFCl_3$	E		X		
10	CFC12	CF_2Cl_2	E		X		
11	CFC13	CCl_2FCClF_2	E		X		
12	CH3CL	CH_3Cl	E		X		
13	CH3BR	CH_3Br	E		X		
14	CH3CCL3	CH_3CCl_3	E		X		
15	CLY		E		X		

GMDD
4, 2199–2278, 2011

Table 3. Continued.

Number	Species name	Formula	Solver	Emissions	Boundary condition	Wet deposition	Dry deposition
16	CL	Cl	I				
17	CL2	Cl_2	I				
18	CLO	ClO	I				
19	CLONO2	$ClONO_2$	I			X	
20	CO2		E		X		
21	OCLO	OClO	I				
22	CL2O2	Cl_2O_2	I				
23	H		I				
24	H2O		I	X			
25	HBR	HBr	I			X	
26	HCFC22	CHF_2Cl	E		X		
27	HCL	HCl	I			X	
28	HOBR	HOBr	I			X	
29	HOCL	HOCl	I			X	
30	N		I				

GMDD
4, 2199–2278, 2011

Table 4. List of reactions.

Tropospheric photolysis	Rate
O2 + hv → 2*O	
O3 + hv → O1D + O2	
O3 + hv → O + O2	
N2O + hv → O1D + N2	
NO + hv → N + O	
NO2 + hv → NO + O	
N2O5 + hv → NO2 + NO3	
N2O5 + hv → NO + O + NO3	
HNO3 + hv → NO2 + OH	
NO3 + hv → NO2 + O	
NO3 + hv → NO + O2	
HO2NO2 + hv → OH + NO3	
HO2NO2 + hv → NO2 + HO2	
CH3OOH + hv → CH2O + H + OH	
CH2O + hv → CO + 2*H	
CH2O + hv → CO + H2	
H2O2 + hv → 2*OH	
CH3CHO + hv → CH3O2 + CO + HO2	
POOH + hv → CH3CHO + CH2O + HO2 + OH	
CH3COOOH + hv → CH3O2 + OH + CO2	
PAN + hv → .6*CH3CO3 + .6*NO2 + .4*CH3O2 + .4*NO3 + .4*CO2	
MPAN + hv → MCO3 + NO2	
MACR + hv → .67*HO2 + .33*MCO3 + .67*CH2O + .67*CH3CO3 + .33*OH + .67*CO	
MVK + hv → .7*C3H6 + .7*CO + .3*CH3O2 + .3*CH3CO3	
C2H5OOH + hv → CH3CHO + HO2 + OH	
C3H7OOH + hv → .82*CH3COCH3 + OH + HO2	
ROOH + hv → CH3CO3 + CH2O + OH	
CH3COCH3 + hv → CH3CO3 + CH3O2	
CH3COCHO + hv → CH3CO3 + CO + HO2	
XOOH + hv → OH	
ONITR + hv → HO2 + CO + NO2 + CH2O	
ISOPOOH + hv → .402*MVK + .288*MACR + .69*CH2O + HO2	
HYAC + hv → CH3CO3 + HO2 + CH2O	
GLYALD + hv → 2*HO2 + CO + CH2O	
MEK + hv → CH3CO3 + C2H5O2	
BIGALD + hv → .45*CO + .13*GLYOXAL + .56*HO2 + .13*CH3CO3 + .18*CH3COCHO	
GLYOXAL + hv → 2*CO + 2*HO2	
ALKOOH + hv → .4*CH3CHO + .1*CH2O + .25*CH3COCH3 + .9*HO2 + .8*MEK + OH	
MEKOOH + hv → OH + CH3CO3 + CH3CHO	
TOLOOH + hv → OH + .45*GLYOXAL + .45*CH3COCHO + .9*BIGALD	
TERPOOH + hv → OH + .1*CH3COCH3 + HO2 + MVK + MACR	

GMDD
4, 2199–2278, 2011

Table 4. Continued.

Stratospheric only photolysis	Rate
CH4 + hv → H + CH3O2	
CH4 + hv → 1.44*H2 + .18*CH2O + .18*O + .66*OH + .44*CO2 + .38*CO + .05*H2O	
H2O + hv → OH + H	
H2O + hv → H2 + O1D	
H2O + hv → 2*H + O	
CL2 + hv → 2*CL	
OCLO + hv → O + CLO	
CL2O2 + hv → 2*CL	
HOCL + hv → OH + CL	
HCL + hv → H + CL	
CLONO2 + hv → CL + NO3	
CLONO2 + hv → CLO + NO2	
BRCL + hv → BR + CL	
BRO + hv → BR + O	
HOBR + hv → BR + OH	
BRONO2 + hv → BR + NO3	
BRONO2 + hv → BRO + NO2	
CH3CL + hv → CL + CH3O2	
CCL4 + hv → 4*CL	
CH3CCL3 + hv → 3*CL	
CFC11 + hv → 3*CL	
CFC12 + hv → 2*CL	
CFC113 + hv → 3*CL	
HCFC22 + hv → CL	
CH3BR + hv → BR + CH3O2	
CF3BR + hv → BR	
CF2CLBR + hv → BR + CL	
CO2 + hv → CO + O	
Odd-Oxygen Reactions	**Rate**
O + O2 + M → O3 + M	6E−34*(300/T)**2.4
O + O3 → 2*O2	8.00E−12*exp(−2060./T)
O + O + M → O2 + M	2.76E−34*exp(720./T)
O1D + N2 → O + N2	2.10E−11*exp(115./T)
O1D + O2 → O + O2	3.20E−11*exp(70./T)
O1D + H2O → 2*OH	2.20E−10
O1D + H2 → HO2 + OH	1.10E−10
O1D + N2O → N2 + O2	4.90E−11
O1D + N2O → 2*NO	6.70E−11
O1D + CH4 → CH3O2 + OH	1.13E−10
O1D + CH4 → CH2O + H + HO2	3.00E−11
O1D + CH4 → CH2O + H2	7.50E−12
O1D + HCN → OH	7.70E−11*exp(100./T)

GMDD
4, 2199–2278, 2011

Table 4. Continued.

Odd hydrogen reactions	Rate
H + O2 + M → HO2 + M	troe : ko=4.40E−32*(300/T)**1.30 ki=4.70E−11*(300/T)**0.20 f=0.60
H + O3 → OH + O2	1.40E−10*exp(−470./T)
H + HO2 → 2*OH	7.20E−11
H + HO2 → H2 + O2	6.90E−12
H + HO2 → H2O + O	1.60E−12
OH + O → H + O2	2.20E−11*exp(120./T)
OH + O3 → HO2 + O2	1.70E−12*exp(−940./T)
OH + HO2 → H2O + O2	4.80E−11*exp(250./T)
OH + OH → H2O + O	1.80E−12
OH + OH + M → H2O2 + M	troe : ko=6.90E−31*(300/T)**1.00 ki=2.60E−11 f=0.60
OH + H2 → H2O + H	2.80E−12*exp(−1800./T)
OH + H2O2 → H2O + HO2	1.80E−12
OH + HCN → HO2	troe : ko=4.28E−33 ki=9.30E−15*(300/T)**−4.42 f=0.80
OH + CH3CN → HO2	7.80E−13*exp(−1050./T)
HO2 + O → OH + O2	3.00E−11*exp(200./T)
HO2 + O3 → OH + 2*O2	1.00E−14*exp(−490./T)
HO2 + HO2 → H2O2 + O2	(2.3E−13*exp(600/T) + 1.7E−33 * [M] * exp(1000/T)) * (1 + 1.4E−21*[H2O]exp(2200/T))
H2O2 + O → OH + HO2	1.40E−12*exp(−2000./T)
Odd nitrogen reactions	**Rate**
N + O2 → NO + O	1.50E−11*exp(−3600./T)
N + NO → N2 + O	2.10E−11*exp(100./T)
N + NO2 → N2O + O	5.80E−12*exp(220./T)
NO + O + M → NO2 + M	troe : ko=9.00E−32*(300/T)**1.50 ki=3.00E−11 f=0.60
NO + HO2 → NO2 + OH	3.50E−12*exp(250./T)
NO + O3 → NO2 + O2	3.00E−12*exp(−1500./T)
NO2 + O → NO + O2	5.10E−12*exp(210./T)
NO2 + O + M → NO3 + M	troe : ko=2.50E−31*(300/T)**1.80 ki=2.20E−11*(300/T)**0.70 f=0.60
NO2 + O3 → NO3 + O2	1.20E−13*exp(−2450./T)
NO2 + NO3 + M → N2O5 + M	troe : ko=2.00E−30*(300/T)**4.40 ki=1.40E−12*(300/T)**0.70 f=0.60
N2O5 + M → NO2 + NO3 + M	k(NO2+NO3+M) * 3.333E26 * exp(10990/T)
NO2 + OH + M → HNO3 + M	troe : ko=1.80E−30*(300/T)**3.00 ki=2.80E−11 f=0.60
HNO3 + OH → NO3 + H2O	k0 + k3[M]/(1 + k3[M]/k2) k0=2.4E−14·exp(460/T) k2=2.7E−17·exp(2199/T) k3=6.5E−34·exp(1335/T)
NO3 + NO → 2*NO2	1.50E−11*exp(170./T)
NO3 + O → NO2 + O2	1.00E−11
NO3 + OH → HO2 + NO2	2.20E−11
NO3 + HO2 → OH + NO2 + O2	3.50E−12

GMDD
4, 2199–2278, 2011

Table 4. Continued.

NO2 + HO2 + M → HO2NO2 + M	troe : ko=2.00E−31*(300/T)**3.40 ki=2.90E−12*(300/T)**1.10 f=0.60
HO2NO2 + OH → H2O + NO2 + O2	1.30E−12*exp(380./T)
HO2NO2 + M → HO2 + NO2 + M	k(NO2+HO2+M)·exp(−10900/T)/2.1E−27
C-1 Degradation (Methane, CO, CH2O and derivatives)	**Rate**
CH4 + OH → CH3O2 + H2O	2.45E−12*exp(−1775./T)
CH3O2 + NO → CH2O + NO2 + HO2	2.80E−12*exp(300./T)
CH3O2 + HO2 → CH3OOH + O2	4.10E−13*exp(750./T)
CH3OOH + OH → CH3O2 + H2O	3.80E−12*exp(200./T)
CH2O + NO3 → CO + HO2 + HNO3	6.00E−13*exp(−2058./T)
CH2O + OH → CO + H2O + H	5.50E−12*exp(125./T)
CH2O + O → HO2 + OH + CO	3.40E−11*exp(−1600./T)
CO + OH + M → CO2 + HO2 + M	troe : ko=5.90E−33*(300/T)**1.40 ki=1.10E−12*(300/T)**−1.30 f=0.60
CO + OH → CO2 + HO2	ki=2.1E09 * (T/300)**6.1 ko=1.5E−13 * (T/300)**0.6 rate=ko/(1+ko/(ki/M)) *0.6**(1/(1+log10(ko/(ki/M)**2)))
CH3O2 + CH3O2 → 2*CH2O + 2*HO2	5.00E−13*exp(−424./T)
CH3O2 + CH3O2 → CH2O + CH3OH	1.90E−14*exp(706./T)
CH3OH + OH → HO2 + CH2O	2.90E−12*exp(−345./T)
CH3OOH + OH → .7*CH3O2 + .3*OH + .3*CH2O + H2O	3.80E−12*exp(200./T)
HCOOH + OH → HO2 + CO2 + H2O	4.50E−13
CH2O + HO2 → HOCH2OO	9.70E−15*exp(625./T)
HOCH2OO → CH2O + HO2	2.40E+12*exp(−7000./T)
HOCH2OO + NO → HCOOH + NO2 + HO2	2.60E−12*exp(265./T)
HOCH2OO + HO2 → HCOOH	7.50E−13*exp(700./T)
C-2 Degradation	**Rate**
C2H2 + OH + M → .65*GLYOXAL + .65*OH + .35*HCOOH + .35*HO2 + .35*CO + M	troe : ko=5.50E−30 ki=8.30E−13*(300/T)**−2.00 f=0.60
C2H6 + OH → C2H5O2 + H2O	8.70E−12*exp(−1070./T)
C2H4 + OH + M → .75*EO2 + .5*CH2O + .25*HO2 + M	troe : ko=1.00E−28*(300/T)**0.80 ki=8.80E−12 f=0.60
C2H4 + O3 → CH2O + .12*HO2 + .5*CO + .12*OH + .5*HCOOH	1.20E−14*exp(−2630./T)
CH3COOH + OH → CH3O2 + CO2 + H2O	7.00E−13
C2H5O2 + NO → CH3CHO + HO2 + NO2	2.60E−12*exp(365./T)
C2H5O2 + HO2 → C2H5OOH + O2	7.50E−13*exp(700./T)
C2H5O2 + CH3O2 → .7*CH2O + .8*CH3CHO + HO2 + .3*CH3OH + .2*C2H5OH	2.00E−13
C2H5O2 + C2H5O2 → 1.6*CH3CHO + 1.2*HO2 + .4*C2H5OH	6.80E−14
C2H5OOH + OH → .5*C2H5O2 + .5*CH3CHO + .5*OH	3.80E−12*exp(200./T)
CH3CHO + OH → CH3CO3 + H2O	5.60E−12*exp(270./T)
CH3CHO + NO3 → CH3CO3 + HNO3	1.40E−12*exp(−1900./T)
CH3CO3 + NO → CH3O2 + CO2 + NO2	8.10E−12*exp(270./T)
CH3CO3 + NO2 + M → PAN + M	troe : ko=8.50E−29*(300/T)**6.50 ki=1.10E−11*(300/T) f=0.60

GMDD
4, 2199–2278, 2011

Table 4. Continued.

CH3CO3 + HO2 → .75*CH3COOOH + .25*CH3COOH + .25*O3	4.30E−13*exp(1040./T)
CH3CO3 + CH3O2 → .9*CH3O2 + CH2O + .9*HO2 + .9*CO2 + .1*CH3COOH	2.00E−12*exp(500./T)
CH3CO3 + CH3CO3 → 2*CH3O2 + 2*CO2	2.50E−12*exp(500./T)
CH3COOOH + OH → .5*CH3CO3 + .5*CH2O + .5*CO2 + H2O	1.00E−12
EO2 + NO → EO + NO2	4.20E−12*exp(180./T)
EO + O2 → GLYALD + HO2	1.00E−14
EO → 2*CH2O + HO2	1.60E+11*exp(−4150./T)
GLYALD + OH → HO2 + .2*GLYOXAL + .8*CH2O + .8*CO2	1.00E−11
GLYOXAL + OH → HO2 + CO + CO2	1.10E−11
C2H5OH + OH → HO2 + CH3CHO	6.90E−12*exp(−230./T)
PAN + M → CH3CO3 + NO2 + M	k(CH3CO3+NO2+M) * 1.111E28 * exp(14000/T)
PAN + OH → CH2O + NO3	4.00E−14
C−3 Degradation	**Rate**
C3H6 + OH + M → PO2 + M	troe : ko=8.00E−27*(300/T)**3.50 ki=3.00E−11 f=0.50
C3H6 + O3 → .54*CH2O + .19*HO2 + .33*OH + .08*CH4 + .56*CO + .5*CH3CHO + .31*CH3O2 + .25*CH3COOH	6.50E−15*exp(−1900./T)
C3H6 + NO3 → ONIT	4.60E−13*exp(−1156./T)
C3H7O2 + NO → .82*CH3COCH3 + NO2 + HO2 + .27*CH3CHO	4.20E−12*exp(180./T)
C3H7O2 + HO2 → C3H7OOH + O2	7.50E−13*exp(700./T)
C3H7O2 + CH3O2 → CH2O + HO2 + .82*CH3COCH3	3.75E−13*exp(−40./T)
C3H7OOH + OH → H2O + C3H7O2	3.80E−12*exp(200./T)
C3H8 + OH → C3H7O2 + H2O	1.00E−11*exp(−665./T)
PO2 + NO → CH3CHO + CH2O + HO2 + NO2	4.20E−12*exp(180./T)
PO2 + HO2 → POOH + O2	7.50E−13*exp(700./T)
POOH + OH → .5*PO2 + .5*OH + .5*HYAC + H2O	3.80E−12*exp(200./T)
CH3COCH3 + OH → RO2 + H2O	3.82E−11 * exp(2000/T) + 1.33E−13
RO2 + NO → CH3CO3 + CH2O + NO2	2.90E−12*exp(300./T)
RO2 + HO2 → ROOH + O2	8.60E−13*exp(700./T)
RO2 + CH3O2 → .3*CH3CO3 + .8*CH2O + .3*HO2 + .2*HYAC + .5*CH3COCHO + .5*CH3OH	7.10E−13*exp(500./T)
ROOH + OH → RO2 + H2O	3.80E−12*exp(200./T)
HYAC + OH → CH3COCHO + HO2	3.00E−12
CH3COCHO + OH → CH3CO3 + CO + H2O	8.40E−13*exp(830./T)
CH3COCHO + NO3 → HNO3 + CO + CH3CO3	1.40E−12*exp(−1860./T)
ONIT + OH → NO2 + CH3COCHO	6.80E−13
C−4 Degradation	**Rate**
BIGENE + OH → ENEO2	5.40E−11
ENEO2 + NO → CH3CHO + .5*CH2O + .5*CH3COCH3 + HO2 + NO2	4.20E−12*exp(180./T)
MVK + OH → MACRO2	4.13E−12*exp(452./T)
MVK + O3 → .8*CH2O + .95*CH3COCHO + .08*OH + .2*O3 + .06*HO2 + .05*CO + .04*CH3CHO	7.52E−16*exp(−1521./T)
MEK + OH → MEKO2	2.30E−12*exp(−170./T)
MEKO2 + NO → CH3CO3 + CH3CHO + NO2	4.20E−12*exp(180./T)
MEKO2 + HO2 → MEKOOH	7.50E−13*exp(700./T)
MEKOOH + OH → MEKO2	3.80E−12*exp(200./T)
MACR + OH → .5*MACRO2 + .5*H2O + .5*MCO3	1.86E−11*exp(175./T)

GMDD
4, 2199–2278, 2011

Table 4. Continued.

MACR + O3 → .8*CH3COCHO + .275*HO2 + .2*CO + .2*O3 + .7*CH2O + .215*OH	4.40E−15*exp(−2500./T)
MACRO2 + NO → NO2 + .47*HO2 + .25*CH2O + .53*GLYALD + .25*CH3COCHO + .53*CH3CO3 + .22*HYAC + .22*CO	2.70E−12*exp(360./T)
MACRO2 + NO → 0.8*ONITR	1.30E−13*exp(360./T)
MACRO2 + NO3 → NO2 + .47*HO2 + .25*CH2O + .25*CH3COCHO + .22*CO + .53*GLYALD + .22*HYAC + .53*CH3CO3	2.40E−12
MACRO2 + HO2 → MACROOH	8.00E−13*exp(700./T)
MACRO2 + CH3O2 → .73*HO2 + .88*CH2O + .11*CO + .24*CH3COCHO + .26*GLYALD + .26*CH3CO3 + .25*CH3OH + .23*HYAC	5.00E−13*exp(400./T)
MACRO2 + CH3CO3 → .25*CH3COCHO + CH3O2 + .22*CO + .47*HO2 + .53*GLYALD + .22*HYAC + .25*CH2O + .53*CH3CO3	1.40E−11
MACROOH + OH → .5*MCO3 + .2*MACRO2 + .1*OH + .2*HO2	2.30E−11*exp(200./T)
MCO3 + NO → NO2 + CH2O + CH3CO3	5.30E−12*exp(360./T)
MCO3 + NO3 → NO2 + CH2O + CH3CO3	5.00E−12
MCO3 + HO2 → .25*O3 + .25*CH3COOH + .75*CH3COOOH + .75*O2	4.30E−13*exp(1040./T)
MCO3 + CH3O2 → 2*CH2O + HO2 + CO2 + CH3CO3	2.00E−12*exp(500./T)
MCO3 + CH3CO3 → 2*CO2 + CH3O2 + CH2O + CH3CO3	4.60E−12*exp(530./T)
MCO3 + MCO3 → 2*CO2 + 2*CH2O + 2*CH3CO3	2.30E−12*exp(530./T)
MCO3 + NO2 + M → MPAN + M	1.1E−11 * 300/T/[M]
MPAN + M → MCO3 + NO2 + M	k(MCO3+NO2+M) * 1.111E28 * exp(14000/T)
MPAN + OH → .5*HYAC + .5*NO3 + .5*CH2O + .5*HO2	troe : ko=8.00E−27*(300/T)**3.50 ki=3.00E−11 f=0.50
C−5 Degradation	**Rate**
ISOP + OH → ISOPO2	2.54E−11*exp(410./T)
ISOP + O3 → .4*MACR + .2*MVK + .07*C3H6 + .27*OH + .06*HO2 + .6*CH2O + .3*CO + .1*O3 + .2*MCO3 + .2*CH3COOH	1.05E−14*exp(−2000./T)
ISOP + NO3 → ISOPNO3	3.03E−12*exp(−446./T)
ISOPO2 + NO → .08*ONITR + .92*NO2 + HO2 + .51*CH2O + .23*MACR + .32*MVK + .37*HYDRALD	4.40E−12*exp(180./T)
ISOPO2 + NO3 → HO2 + NO2 + .6*CH2O + .25*MACR + .35*MVK + .4*HYDRALD	2.40E−12
ISOPO2 + HO2 → ISOPOOH	8.00E−13*exp(700./T)
ISOPOOH + OH → .8*XO2 + .2*ISOPO2	1.52E−11*exp(200./T)
ISOPO2 + CH3O2 → .25*CH3OH + HO2 + 1.2*CH2O + .19*MACR + .26*MVK + .3*HYDRALD	5.00E−13*exp(400./T)
ISOPO2 + CH3CO3 → CH3O2 + HO2 + .6*CH2O + .25*MACR + .35*MVK + .4*HYDRALD	1.40E−11
ISOPNO3 + NO → 1.206*NO2 + .794*HO2 + .072*CH2O + .167*MACR + .039*MVK + .794*ONITR	2.70E−12*exp(360./T)
ISOPNO3 + NO3 → 1.206*NO2 + .072*CH2O + .167*MACR + .039*MVK + .794*ONITR + .794*HO2	2.40E−12
ISOPNO3 + HO2 → XOOH + .206*NO2 + .794*HO2 + .008*CH2O + .167*MACR + .039*MVK + .794*ONITR	8.00E−13*exp(700./T)
BIGALK + OH → ALKO2	3.50E−12
ONITR + OH → HYDRALD + .4*NO2 + HO2	4.50E−11
ONITR + NO3 → HO2 + NO2 + HYDRALD	1.40E−12*exp(−1860./T)
HYDRALD + OH → XO2	1.86E−11*exp(175./T)
ALKO2 + NO → .4*CH3CHO + .1*CH2O + .25*CH3COCH3 + .9*HO2 + .8*MEK + .9*NO2 + .1*ONIT	4.20E−12*exp(180./T)
ALKO2 + HO2 → ALKOOH	7.50E−13*exp(700./T)

GMDD
4, 2199–2278, 2011

Table 4. Continued.

ALKOOH + OH → ALKO2	3.80E−12*exp(200./T)
XO2 + NO → NO2 + HO2 + .5*CO + .25*GLYOXAL + .25*HYAC + .25*CH3COCHO + .25*GLYALD	2.70E−12*exp(360./T)
XO2 + NO3 → NO2 + HO2 + 0.5*CO + .25*HYAC + 0.25*GLYOXAL + .25*CH3COCHO + .25*GLYALD	2.40E−12
XO2 + HO2 → XOOH	8.00E−13*exp(700./T)
XO2 + CH3O2 → .3*CH3OH + 0.8*HO2 + .7*CH2O + .2*CO + .1*HYAC + .1*GLYOXAL + .1*CH3COCHO + .1*GLYALD	5.00E−13*exp(400./T)
XO2 + CH3CO3 → 0.5*CO + CH3O2 + HO2 + CO2 + .25*GLYOXAL + .25*HYAC + .25*CH3COCHO + .25*GLYALD	1.30E−12*exp(640./T)
XOOH + OH → H2O + XO2	1.90E−12*exp(190./T)
XOOH + OH → H2O + OH	T**2 * 7.69E−17 * exp(253/T)
C-7 Degradation	Rate
TOLUENE + OH → .25*CRESOL + .25*HO2 + .7*TOLO2	1.70E−12*exp(352./T)
TOLO2 + NO → .45*GLYOXAL + .45*CH3COCHO + .9*BIGALD + .9*NO2 + .9*HO2	4.20E−12*exp(180./T)
TOLO2 + HO2 → TOLOOH	7.50E−13*exp(700./T)
TOLOOH + OH → TOLO2	3.80E−12*exp(200./T)
CRESOL + OH → XOH	3.00E−12
XOH + NO2 → .7*NO2 + .7*BIGALD + .7*HO2	1.00E−11
C-10 Degradation	Rate
C10H16 + OH → TERPO2	1.20E−11*exp(444./T)
C10H16 + O3 → .7*OH + MVK + MACR + HO2	1.00E−15*exp(−732./T)
C10H16 + NO3 → TERPO2 + NO2	1.20E−12*exp(490./T)
TERPO2 + NO → .1*CH3COCH3 + HO2 + MVK + MACR + NO2	4.20E−12*exp(180./T)
TERPO2 + HO2 → TERPOOH	7.50E−13*exp(700./T)
TERPOOH + OH → TERPO2	3.80E−12*exp(200./T)
Radon/Lead	Rate
Rn → Pb	2.10E−06
Aerosol precursors and aging	Rate
SO2+ OH → SO4	ko=3.0E−31(300/T)3.3; ki=1.E−12; f=0.6
DMS + OH → SO2	9.60E−12*exp(−234./T)
DMS + OH → .5*SO2+ .5*HO2	1.7E−42 * exp(7810/T) * [M] * 0.21/ (1 + 5.5E−31 * exp(7460/T)* [M] * 0.21)
DMS + NO3 → SO2+ HNO3	1.90E−13*exp(520./T)
NH3 + OH → H2O	1.70E−12*exp(−710./T)
CB1 → CB2	7.10E−06
OC1 → OC2	7.10E−06

GMDD
4, 2199–2278, 2011

Table 4. Continued.

Heterogeneous reactions on tropospheric aerosols	Rate : γ=reaction probability
N2O5 → 2*HNO3	γ=0.1 on OC, SO4, NH4NO3, SOA
NO3 → HNO3	γ=0.001 on OC, SO4, NH4NO3, SOA
NO2 → 0.5*OH + 0.5*NO + 0.5*HNO3	γ=0.0001 on OC, SO4, NH4NO3, SOA
HO2 → 0.5*H2O2	γ=0.2 on OC, SO4, NH4NO3, SOA
O1D reactions with halogens	**Rate**
O1D + CFC11 → 3*CL	1.70E−10
O1D + CFC12 → 2*CL	1.20E−10
O1D + CFC113 → 3*CL	1.50E−10
O1D + HCFC22 → CL	7.20E−11
O1D + CCL4 → 4*CL	2.84E−10
O1D + CH3BR → BR	1.80E−10
O1D + CF2CLBR → BR	9.60E−11
O1D + CF3BR → BR	4.10E−11
Odd Chlorine Reactions	**Rate**
CL + O3 → CLO + O2	2.30E−11*exp(−200./T)
CL + H2 → HCL + H	3.05E−11*exp(−2270./T)
CL + H2O2 → HCL + HO2	1.10E−11*exp(−980./T)
CL + HO2 → HCL + O2	1.80E−11*exp(170./T)
CL + HO2 → OH + CLO	4.10E−11*exp(−450./T)
CL + CH2O → HCL + HO2 + CO	8.10E−11*exp(−30./T)
CL + CH4 → CH3O2 + HCL	7.30E−12*exp(−1280./T)
CLO + O → CL + O2	2.80E−11*exp(85./T)
CLO + OH → CL + HO2	7.40E−12*exp(270./T)
CLO + OH → HCL + O2	6.00E−13*exp(230./T)
CLO + HO2 → O2 + HOCL	2.70E−12*exp(220./T)
CLO + NO → NO2 + CL	6.40E−12*exp(290./T)
CLO + NO2 + M → CLONO2 + M	troe : ko=1.80E−31*(300/T)**3.40 ki=1.50E−11*(300/T)**1.90 f=0.60
CLO + CLO → 2*CL + O2	3.00E−11*exp(−2450./T)
CLO + CLO → CL2 + O2	1.00E−12*exp(−1590./T)
CLO + CLO → CL + OCLO	3.50E−13*exp(−1370./T)
CLO + CLO + M → CL2O2 + M	troe : ko=1.60E−32*(300/T)**4.50 ki=2.00E−12*(300/T)**2.40 f=0.60
CL2O2 + M → CLO + CLO + M	** User defined **
HCL + OH → H2O + CL	2.60E−12*exp(−350./T)
HCL + O → CL + OH	1.00E−11*exp(−3300./T)
HOCL + O → CLO + OH	1.70E−13
HOCL + CL → HCL + CLO	2.50E−12*exp(−130./T)
HOCL + OH → H2O + CLO	3.00E−12*exp(−500./T)
CLONO2 + O → CLO + NO3	2.90E−12*exp(−800./T)
CLONO2 + OH → HOCL + NO3	1.20E−12*exp(−330./T)
CLONO2 + CL → CL2 + NO3	6.50E−12*exp(135./T)

GMDD
4, 2199–2278, 2011

Table 4. Continued.

Odd Bromine Reactions	Rate
BR + O3 → BRO + O2	1.70E−11*exp(−800./T)
BR + HO2 → HBR + O2	4.80E−12*exp(−310./T)
BR + CH2O → HBR + HO2 + CO	1.70E−11*exp(−800./T)
BRO + O → BR + O2	1.90E−11*exp(230./T)
BRO + OH → BR + HO2	1.70E−11*exp(250./T)
BRO + HO2 → HOBR + O2	4.50E−12*exp(460./T)
BRO + NO → BR + NO2	8.80E−12*exp(260./T)
BRO + NO2 + M → BRONO2 + M	troe : ko=5.20E−31*(300/T)**3.20 ki=6.90E−12*(300/T)**2.90 f=0.60
BRO + CLO → BR + OCLO	9.50E−13*exp(550./T)
BRO + CLO → BR + CL + O2	2.30E−12*exp(260./T)
BRO + CLO → BRCL + O2	4.10E−13*exp(290./T)
BRO + BRO → 2*BR + O2	1.50E−12*exp(230./T)
HBR + OH → BR + H2O	5.50E−12*exp(200./T)
HBR + O → BR + OH	5.80E−12*exp(−1500./T)
HOBR + O → BRO + OH	1.20E−10*exp(−430./T)
BRONO2 + O → BRO + NO3	1.90E−11*exp(215./T)
Organic Halogens Reactions with Cl, OH	**Rate**
CH3CL + CL → HO2 + CO + 2*HCL	2.17E−11*exp(−1130./T)
CH3CL + OH → CL + H2O + HO2	2.40E−12*exp(−1250./T)
CH3CCL3 + OH → H2O + 3*CL	1.64E−12*exp(−1520./T)
HCFC22 + OH → CL + H2O + CF2O	1.05E−12*exp(−1600./T)
CH3BR + OH → BR + H2O + HO2	2.35E−12*exp(−1300./T)
Sulfate aerosol reactions	**Comment**
N2O5 → 2*HNO3	γ=0.04
CLONO2 → HOCL + HNO3	f (sulfuric acid wt%)
BRONO2 → HOBR + HNO3	f (T, P, HCl, H2O, r)
CLONO2 + HCL → CL2 + HNO3	f (T, P, H2O, r)
HOCL + HCL → CL2 + H2O	f (T, P, HCl, H2O, r)
HOBR + HCL → BRCL + H2O	f (T, P, HCl, HOBr,H2O, r)
Nitric acid di−hydrate reactions	**Comment**
N2O5 → 2*HNO3	γ=0.0004
CLONO2 → HOCL + HNO3	γ=0.004
CLONO2 + HCL → CL2 + HNO3	γ=0.2
HOCL + HCL → CL2 + H2O	γ=0.1
BRONO2 → HOBR + HNO3	γ=0.3

GMDD
4, 2199–2278, 2011

Table 4. Continued.

Ice aerosol reactions	Comment
N2O5 → 2*HNO3	γ=0.02
CLONO2 → HOCL + HNO3	γ=0.3
BRONO2 → HOBR + HNO3	γ=0.3
CLONO2 + HCL → CL2 + HNO3	γ=0.3
HOCL + HCL → CL2 + H2O	γ=0.2
HOBR + HCL → BRCL + H2O	γ=0.3

GMDD
4, 2199–2278, 2011

Table 5. Bulk aerosol parameters used in calculation of surface area: number distribution mean radius (rm), geometric standard deviation (σg) and density.

Aerosol	rm (nm)	σg (µm)	ρ (g cm^{-3})
CB1, CB2	11.8	2.00	1.0
OC1, OC2	21.2	2.20	1.8
SO4	69.5	2.03	1.7
NH4NO3	69.5	2.03	1.7
SOA	21.2	2.20	1.8

GMDD
4, 2199–2278, 2011

Table 6. Summary of simulations. All versions extend to ≈40 km.

Name	Dynamics	Period	Chemistry	Resolution	Levels
Online strat-trop	online	1991–2000	stratosphere-troposphere	1.9°×2.5°	26
Offline GEOS	GEOS5	2004–2010	troposphere	1.9°×2.5°	56
Offline MERRA	MERRA	1997–2010	troposphere	1.9°×2.5°	56

GMDD
4, 2199–2278, 2011

Table 7. Yearly emission totals (Tg(species)/yr).

Species	Sector	1997	1998	1999	2000	2001	2002	2002	2004	2005	2006	2007	2008	2009	2010
BIGALK	anthro	73.3	73.6	73.9	74.3	74.8	75.3	75.9	76.5	77.0	77.6	78.2	78.8	78.8	78.8
	bb	1.9	2.1	1.4	1.2	1.3	1.5	1.4	1.4	1.4	1.4	1.4	1.1	0.8	0.8
	total	75.2	75.7	75.3	75.5	76.0	76.8	77.3	77.9	78.5	79.0	79.6	79.9	79.5	79.6
BIGENE	anthro	7.1	7.1	7.1	7.2	7.3	7.4	7.5	7.5	7.6	7.7	7.7	7.8	7.8	7.8
	bb	2.3	2.3	1.2	0.9	1.0	1.4	1.3	1.4	1.4	1.4	1.4	0.9	2.0	2.1
	total	9.5	9.5	8.4	8.1	8.2	8.8	8.8	8.9	9.0	9.1	9.1	8.6	9.8	9.9
C10H16	biogenic	81.3	81.3	81.3	81.3	81.3	81.3	81.3	81.3	81.3	81.3	81.3	81.3	81.3	81.3
C2H2	anthro	3.4	3.4	3.4	3.4	3.4	3.4	3.4	3.4	3.4	3.4	3.4	3.4	3.4	3.4
	bb	0.3	0.3	0.2	0.2	0.2	0.2	0.2	0.2	0.3	0.2	0.2	0.2	0.7	0.7
	total	3.8	3.8	3.7	3.6	3.6	3.7	3.7	3.7	3.7	3.7	3.7	3.6	4.1	4.2
C2H4	anthro	6.7	6.7	6.7	6.7	6.8	7.0	7.1	7.2	7.2	7.3	7.4	7.5	7.5	7.5
	bb	8.8	8.4	5.6	4.6	5.1	5.8	5.4	6.0	6.1	5.8	6.0	4.3	3.0	3.1
	biogenic	5.0	5.0	5.0	5.0	5.0	5.0	5.0	5.0	5.0	5.0	5.0	5.0	5.0	5.0
	total	20.4	20.1	17.2	16.3	16.9	17.8	17.4	18.2	18.4	18.1	18.4	16.8	15.4	15.6
C2H5OH	anthro	5.4	5.4	5.4	5.4	5.4	5.4	5.4	5.4	5.4	5.4	5.4	5.4	5.4	5.4
	bb	0.6	0.6	0.4	0.4	0.4	0.5	0.4	0.5	0.5	0.4	0.5	0.4	0.0	0.0
	total	6.0	6.0	5.8	5.8	5.8	5.8	5.8	5.8	5.8	5.8	5.8	5.7	5.4	5.4
C2H6	anthro	7.5	7.5	7.5	7.5	7.6	7.6	7.7	7.7	7.8	7.8	7.9	7.9	7.9	7.9
	bb	4.9	4.5	2.8	2.3	2.5	3.0	2.7	3.2	3.2	3.1	3.1	2.1	1.7	1.9
	biogenic	1.0	1.0	1.0	1.0	1.0	1.0	1.0	1.0	1.0	1.0	1.0	1.0	1.0	1.0
	total	13.4	13.0	11.4	10.8	11.1	11.6	11.4	11.9	12.0	11.9	12.0	11.0	10.6	10.7
C3H6	anthro	2.8	2.8	2.8	2.8	2.8	2.9	2.9	2.9	3.0	3.0	3.0	3.1	3.1	3.1
	bb	2.6	2.8	1.8	1.5	1.6	1.9	1.9	1.9	1.9	1.8	1.9	1.4	1.6	1.8
	biogenic	1.0	1.0	1.0	1.0	1.0	1.0	1.0	1.0	1.0	1.0	1.0	1.0	1.0	1.0
	total	6.4	6.6	5.5	5.3	5.5	5.8	5.8	5.8	5.9	5.8	5.9	5.5	5.7	5.8
C3H8	anthro	7.9	8.0	8.0	8.0	8.1	8.2	8.2	8.3	8.3	8.4	8.5	8.5	8.5	8.5
	bb	0.8	0.9	0.6	0.5	0.5	0.6	0.6	0.6	0.6	0.6	0.6	0.5	0.4	0.4
	biogenic	2.0	2.0	2.0	2.0	2.0	2.0	2.0	2.0	2.0	2.0	2.0	2.0	2.0	2.0
	total	10.7	10.8	10.5	10.5	10.6	10.8	10.8	10.9	10.9	11.0	11.0	11.0	10.9	10.9
CB1	anthro	3.7	3.7	3.7	3.7	3.7	3.7	3.7	3.7	3.7	3.7	3.7	3.7	3.7	3.7
	bb	2.9	3.0	2.1	1.8	2.0	2.2	2.0	2.1	2.2	2.0	2.2	1.7	1.7	1.8
	total	6.6	6.7	5.8	5.5	5.7	5.9	5.8	5.9	5.9	5.8	5.9	5.4	5.4	5.5
CB2	anthro	0.9	0.9	0.9	0.9	0.9	0.9	0.9	0.9	0.9	0.9	0.9	0.9	0.9	0.9
	bb	0.7	0.8	0.5	0.5	0.5	0.5	0.5	0.5	0.5	0.5	0.5	0.4	0.4	0.4
	total	1.7	1.7	1.5	1.4	1.4	1.5	1.4	1.5	1.5	1.4	1.5	1.4	1.3	1.4
CH2O	anthro	0.9	0.9	0.9	1.0	1.0	1.0	1.0	1.0	1.0	1.1	1.1	1.1	1.1	1.1
	bb	4.2	4.9	2.7	2.2	2.3	3.1	3.1	2.8	2.8	2.9	2.8	2.1	4.4	4.7
	total	5.1	5.8	3.6	3.2	3.3	4.1	4.1	3.9	3.9	4.0	3.9	3.2	5.5	5.8
CH3CHO	anthro	2.1	2.1	2.1	2.1	2.2	2.2	2.2	2.2	2.2	2.2	2.2	2.2	2.2	2.2
	bb	7.6	8.2	5.5	4.8	5.1	5.8	5.6	5.6	5.7	5.4	5.7	4.5	4.6	4.7
	total	9.8	10.3	7.6	6.9	7.3	8.0	7.8	7.8	7.9	7.6	7.9	6.7	6.9	7.0
CH3CN	biofuel	0.7	0.7	0.7	0.7	0.7	0.7	0.7	0.7	0.7	0.7	0.7	0.7	0.7	0.7
	bb	1.6	1.7	1.1	1.0	1.1	1.2	1.2	1.2	1.2	1.1	1.2	0.9	1.1	1.2
	total	2.3	2.4	1.9	1.7	1.8	1.9	1.9	1.9	1.9	1.9	1.9	1.6	1.8	1.9
CH3COCH3	anthro	0.3	0.3	0.3	0.3	0.3	0.3	0.3	0.3	0.3	0.3	0.3	0.3	0.3	0.3
	bb	3.4	3.6	2.5	2.2	2.4	2.6	2.4	2.6	2.6	2.4	2.6	2.0	1.9	2.0
	biogenic	24.3	24.3	24.3	24.3	24.3	24.3	24.3	24.3	24.3	24.3	24.3	24.3	24.3	24.3
	total	28.1	28.2	27.1	26.8	27.0	27.3	27.1	27.2	27.3	27.1	27.3	26.7	26.6	26.7

GMDD
4, 2199–2278, 2011

Table 7. Continued.

species	sector	1997	1998	1999	2000	2001	2002	2002	2004	2005	2006	2007	2008	2009	2010
CH3COOH	anthro	6.6	6.6	6.6	6.6	6.6	6.6	6.6	6.6	6.6	6.6	6.6	6.6	6.6	6.6
	bb	3.1	2.7	1.8	1.5	1.5	2.0	1.9	2.0	2.2	2.1	2.1	1.6	8.1	8.5
	total	9.7	9.3	8.4	8.2	8.1	8.6	8.6	8.6	8.8	8.7	8.7	8.2	14.7	15.1
CH3OH	anthro	0.4	0.4	0.4	0.4	0.4	0.4	0.4	0.4	0.4	0.4	0.4	0.4	0.4	0.4
	bb	10.7	11.3	7.6	6.7	7.2	8.1	7.7	7.9	8.0	7.6	8.0	6.2	5.7	6.1
	biogenic	228.8	228.8	228.8	228.8	228.8	228.8	228.8	228.8	228.8	228.8	228.8	228.8	228.8	228.8
	total	239.9	240.5	236.8	235.8	236.4	237.3	236.9	237.1	237.2	236.8	237.2	235.4	234.9	235.3
CO	anthro	598.0	595.3	595.0	598.8	607.0	620.9	631.5	635.1	638.8	642.5	646.1	649.8	649.8	649.8
	bb	552.9	586.6	388.5	334.8	363.0	415.3	394.1	403.0	408.7	387.5	406.9	313.3	351.8	378.1
	biogenic	159.3	159.3	159.3	159.3	159.3	159.3	159.3	159.3	159.3	159.3	159.3	159.3	159.3	159.3
	ocean	19.8	19.8	19.8	19.8	19.8	19.8	19.8	19.8	19.8	19.8	19.8	19.8	19.8	19.8
	total	1330.1	1361.0	1162.6	1112.7	1149.1	1215.4	1204.8	1217.3	1226.7	1209.1	1232.2	1142.3	1180.8	1207.1
DMS	ocean	59.9	59.9	59.9	59.9	59.9	59.9	59.9	59.9	59.9	59.9	59.9	59.9	59.9	59.9
HCN	biofuel	1.0	1.0	1.0	1.0	1.0	1.0	1.0	1.0	1.0	1.0	1.0	1.0	1.0	1.0
	bb	2.2	2.4	1.6	1.4	1.5	1.7	1.6	1.6	1.7	1.6	1.6	1.3	1.3	1.4
	total	3.2	3.4	2.6	2.3	2.5	2.7	2.6	2.6	2.6	2.6	2.6	2.3	2.3	2.4
HCOOH	anthro	6.6	6.6	6.6	6.6	6.6	6.6	6.6	6.6	6.6	6.6	6.6	6.6	6.6	6.6
	bb	0.6	0.6	0.4	0.3	0.3	0.4	0.4	0.4	0.4	0.4	0.4	0.3	1.7	1.7
	total	7.2	7.2	7.0	6.9	6.9	7.0	7.0	7.0	7.1	7.0	7.0	7.0	8.3	8.3
ISOP	biogenic	534.9	534.9	534.9	534.9	534.9	534.9	534.9	534.9	534.9	534.9	534.9	534.9	534.9	534.9
MEK	anthro	1.2	1.2	1.2	1.3	1.3	1.3	1.3	1.3	1.3	1.4	1.4	1.4	1.4	1.4
	bb	7.4	7.9	5.2	4.5	4.9	5.6	5.3	5.4	5.5	5.2	5.5	4.2	4.7	5.0
	total	8.6	9.1	6.5	5.8	6.2	6.9	6.6	6.8	6.9	6.6	6.8	5.7	6.1	6.4
NH3	anthro	47.9	48.2	48.6	48.8	48.9	49.0	49.3	49.7	50.2	50.7	51.1	51.6	51.6	51.6
	bb	7.9	8.5	5.9	5.2	5.6	6.2	5.9	6.0	6.1	5.7	6.1	4.8	4.2	4.6
	ocean	8.1	8.1	8.1	8.1	8.1	8.1	8.1	8.1	8.1	8.1	8.1	8.1	8.1	8.1
	soil	2.4	2.4	2.4	2.4	2.4	2.4	2.4	2.4	2.4	2.4	2.4	2.4	2.4	2.4
	total	66.3	67.2	65.0	64.5	65.1	65.7	65.7	66.3	66.9	66.9	67.7	67.0	66.3	66.7
NO	anthro	59.3	59.7	60.3	60.9	61.6	62.9	63.9	64.4	64.9	65.4	65.9	66.5	66.5	66.5
	bb	14.0	16.0	11.4	10.4	11.1	12.0	11.6	11.3	11.5	10.7	11.5	9.7	5.5	5.9
	soil	17.1	17.1	17.1	17.1	17.1	17.1	17.1	17.1	17.1	17.1	17.1	17.1	17.1	17.1
	total	90.4	92.8	88.7	88.3	89.8	91.9	92.6	92.8	93.5	93.2	94.5	93.2	89.0	89.4
OC1	anthro	8.1	8.1	8.1	8.1	8.1	8.1	8.1	8.1	8.1	8.1	8.1	8.1	8.1	8.1
	bb	14.5	17.1	10.6	9.2	9.7	11.7	11.6	10.7	10.8	10.6	10.9	8.7	10.9	11.8
	total	22.5	25.1	18.6	17.3	17.8	19.8	19.7	18.8	18.8	18.6	18.9	16.8	19.0	19.8
OC2	anthro	8.1	8.1	8.1	8.1	8.1	8.1	8.1	8.1	8.1	8.1	8.1	8.1	8.1	8.1
	bb	14.5	17.1	10.6	9.2	9.7	11.7	11.6	10.7	10.8	10.6	10.9	8.7	10.9	11.8
	total	22.5	25.1	18.6	17.3	17.8	19.8	19.7	18.8	18.8	18.6	18.9	16.8	19.0	19.8
SO2	anthro	129.0	128.6	128.8	130.3	132.8	136.7	139.2	139.2	139.1	139.1	139.0	139.0	139.0	139.0
	bb	3.2	3.7	2.3	2.0	2.1	2.6	2.5	2.3	2.4	2.3	2.4	1.9	2.3	2.5
	volcano	9.5	9.5	9.5	9.5	9.5	9.5	9.5	9.5	9.5	9.5	9.5	9.5	9.5	9.5
	total	141.7	141.9	140.7	141.9	144.5	148.8	151.3	151.1	151.0	150.9	150.9	150.4	150.8	151.0
TOLUENE	anthro	28.7	28.8	29.0	29.2	29.5	30.0	30.4	30.8	31.2	31.6	32.0	32.4	32.4	32.4
	bb	3.8	4.5	2.8	2.5	2.6	3.1	3.1	2.9	2.9	2.8	2.9	2.3	11.8	12.6
	total	32.5	33.3	31.8	31.7	32.2	33.1	33.5	33.7	34.1	34.4	34.9	34.7	44.2	45.0

GMDD
4, 2199–2278, 2011

CAM-chem description and evaluation

J.-F. Lamarque et al.

Table 8. Tropospheric (ozone ≤ 100 ppb) ozone budget: all terms in Tg yr^{-1}.

Name	Burden	Net chemistry	Deposition	STE
Offline GEOS5/MERRA	296.5	206.7	704.2	497.5
Online strat-trop	296.4	330.7	739.4	408.7

GMDD
4, 2199–2278, 2011

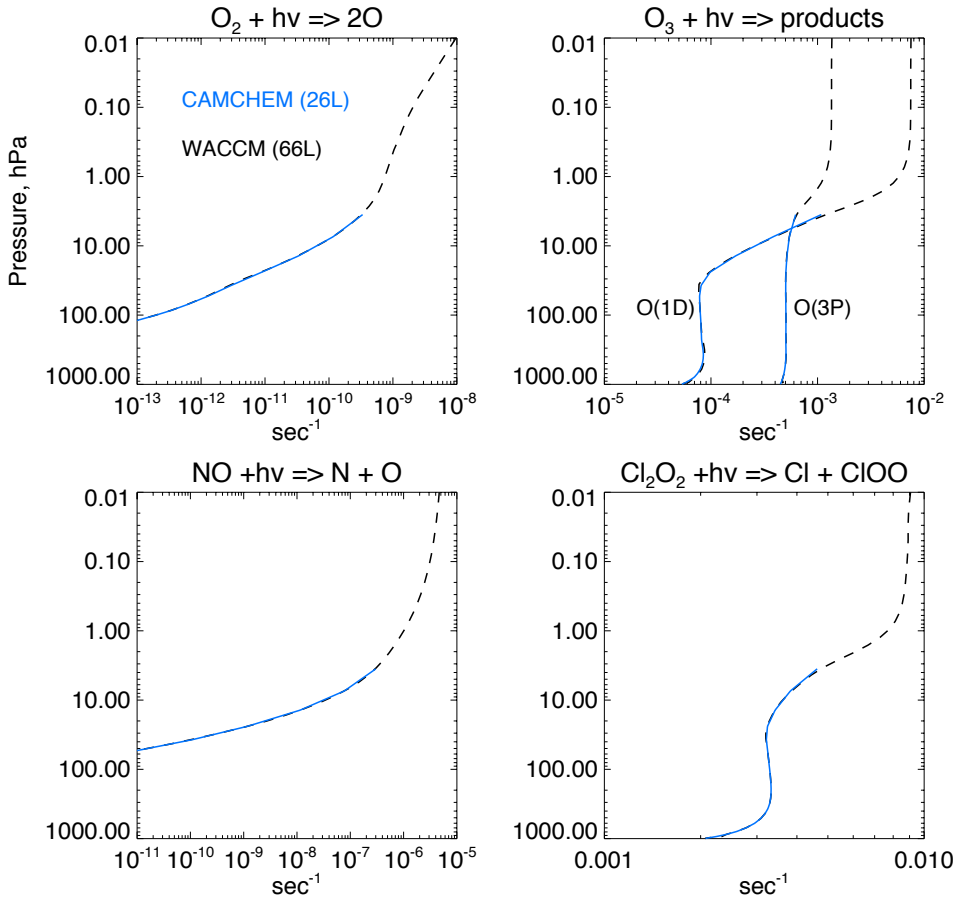

Fig. 1. Photolysis rates in CAM and WACCM for 1 January, noon at 0° N conditions.

GMDD
4, 2199–2278, 2011

CAM-chem description and evaluation

J.-F. Lamarque et al.

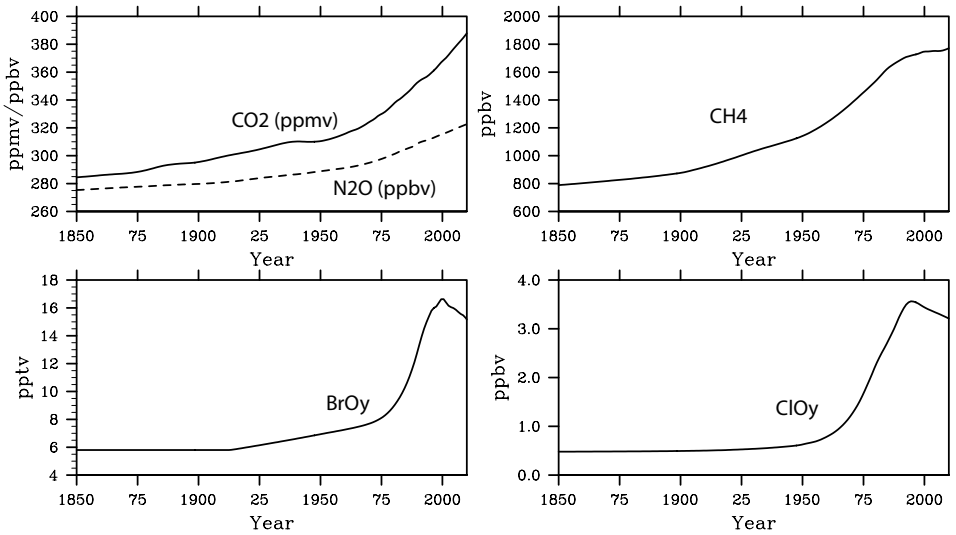

Fig. 2. Time evolution of long-lived chemical species (from Meinshausen et al., 2011) specified as lower boundary condition (see Table 3). In addition, H_2 is fixed at 500 pptv.

GMDD
4, 2199–2278, 2011

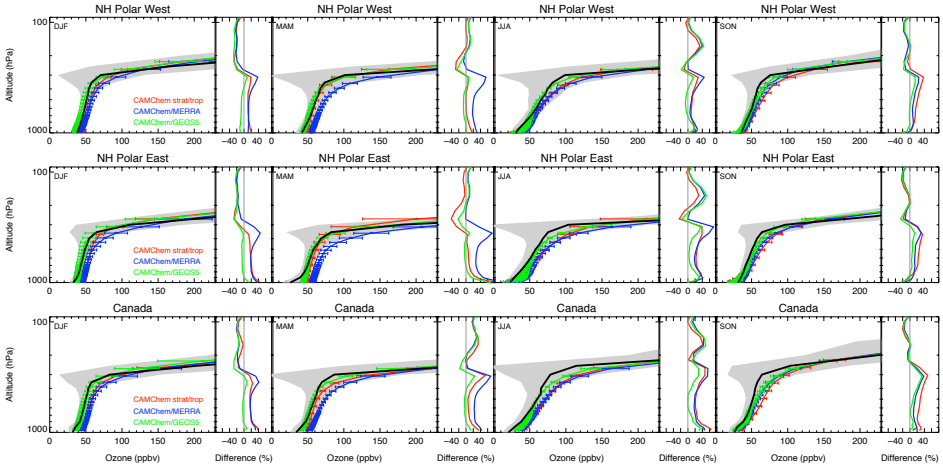

Fig. 3. Regionally-aggregated (see Fig. S2 for definition) median ozonesonde profiles for each season (winter, left column; spring, second column; summer, third column, fall; right column). In each panel, the bias with respect to the observation median is shown as relative difference.

GMDD
4, 2199–2278, 2011

CAM-chem description and evaluation

J.-F. Lamarque et al.

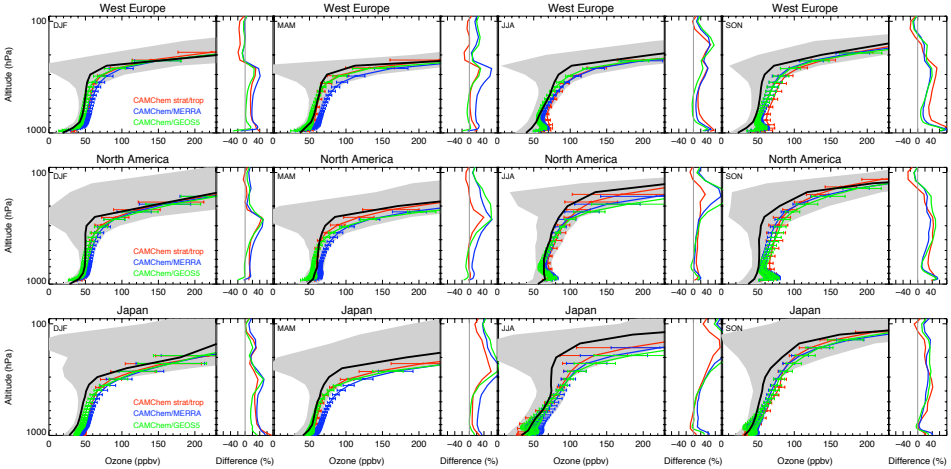

Fig. 3. Continued.

GMDD
4, 2199–2278, 2011

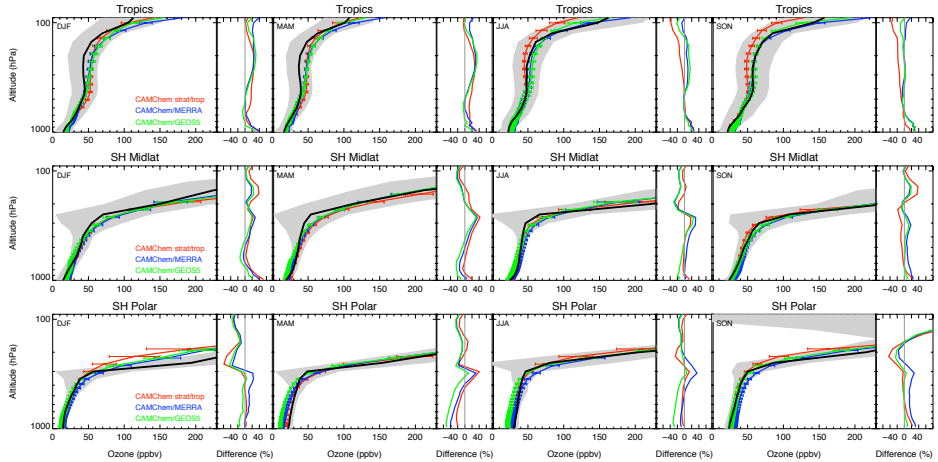

Fig. 3. Continued.

GMDD
4, 2199–2278, 2011

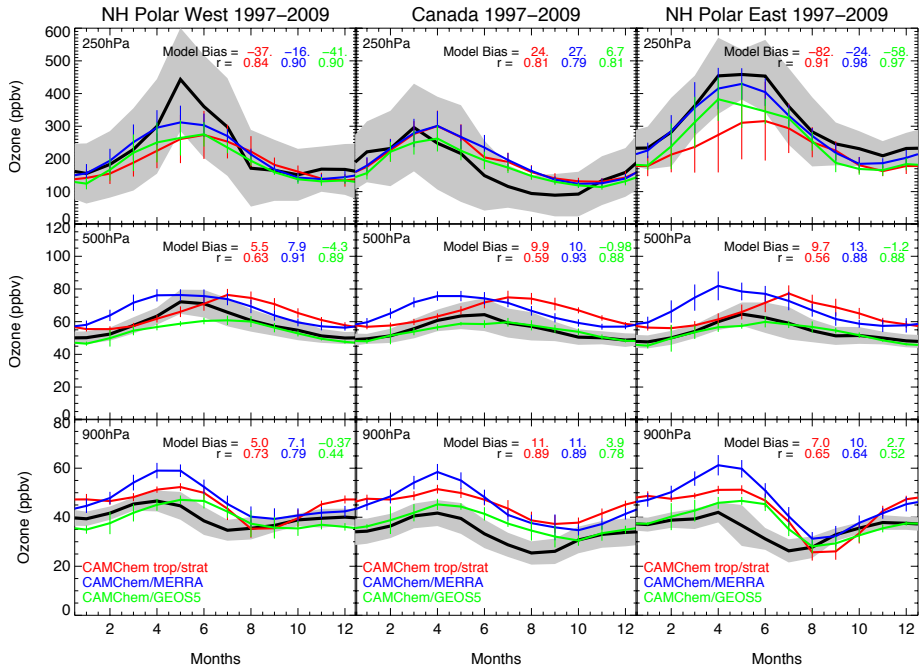

Fig. 4. Comparison of the mean seasonal cycle for regionally-aggregated stations. Observations and model simulations cover 1997–2009, except for the GEOS5 simulation which starts in 2004.

GMDD
4, 2199–2278, 2011

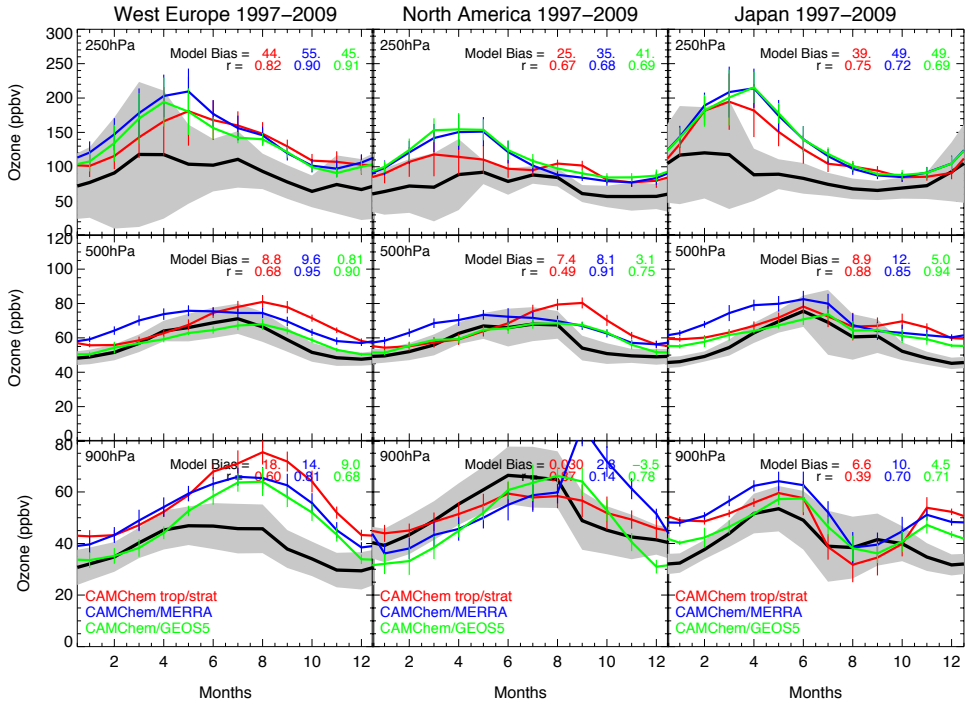

Fig. 4. Continued.

GMDD
4, 2199–2278, 2011

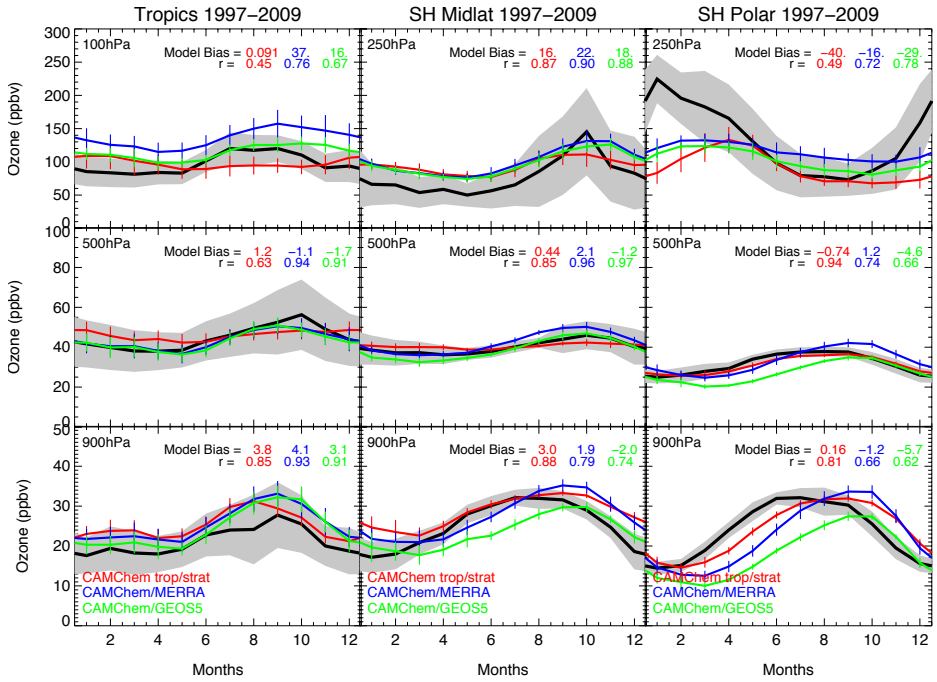

Fig. 4. Continued.

GMDD
4, 2199–2278, 2011

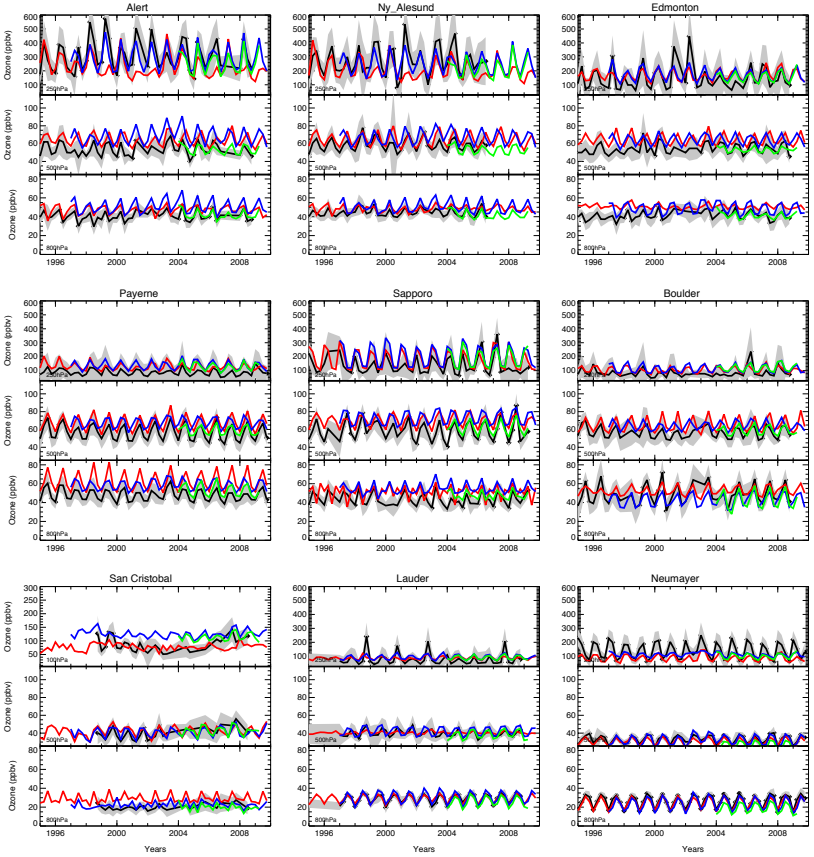

Fig. 5. Long-term change in median observed (grey shading indicates variability within the season) and simulated tropospheric ozone (250 hPa, 500 hPa and 800 hPa) for a variety of stations spanning the globe. Seasonal averages are shown. Black line is observations, red line is online, blue line is GEOS5 and green line is MERRA.

GMDD
4, 2199–2278, 2011

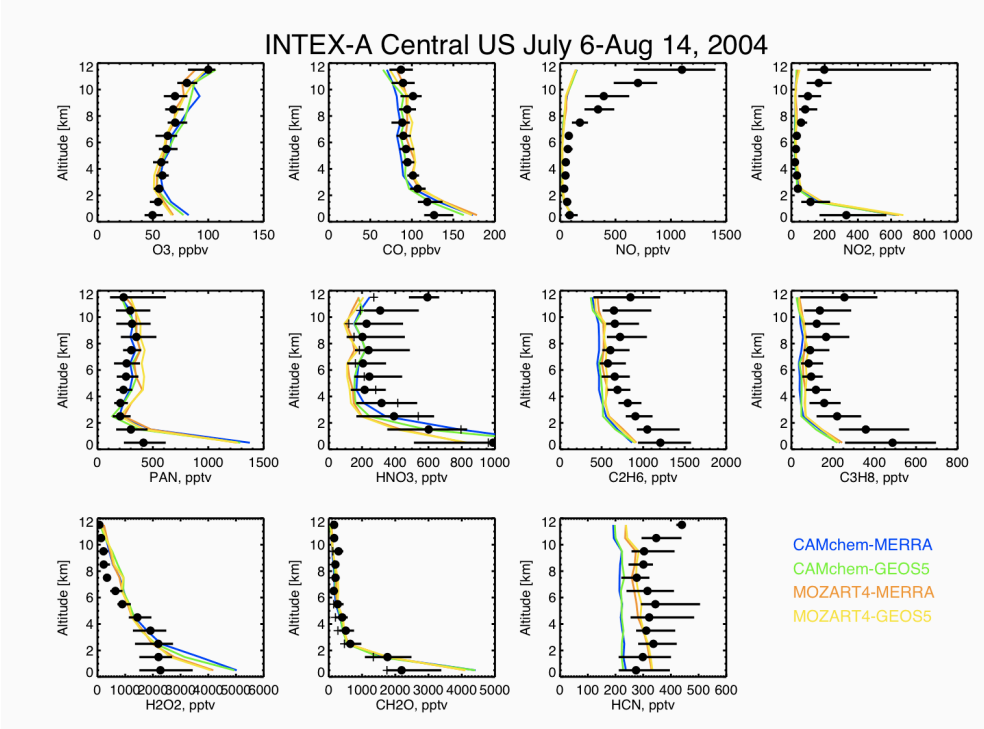

Fig. 6a. Comparison of specified-dynamics simulations with INTEX-A Central US for selected aircraft observations. All flights in the considered period are aggregated and variability is shown as horizontal line. Additional MOZART-4 simulations with the same emissions and meteorological fields are shown as yellow and orange.

GMDD
4, 2199–2278, 2011

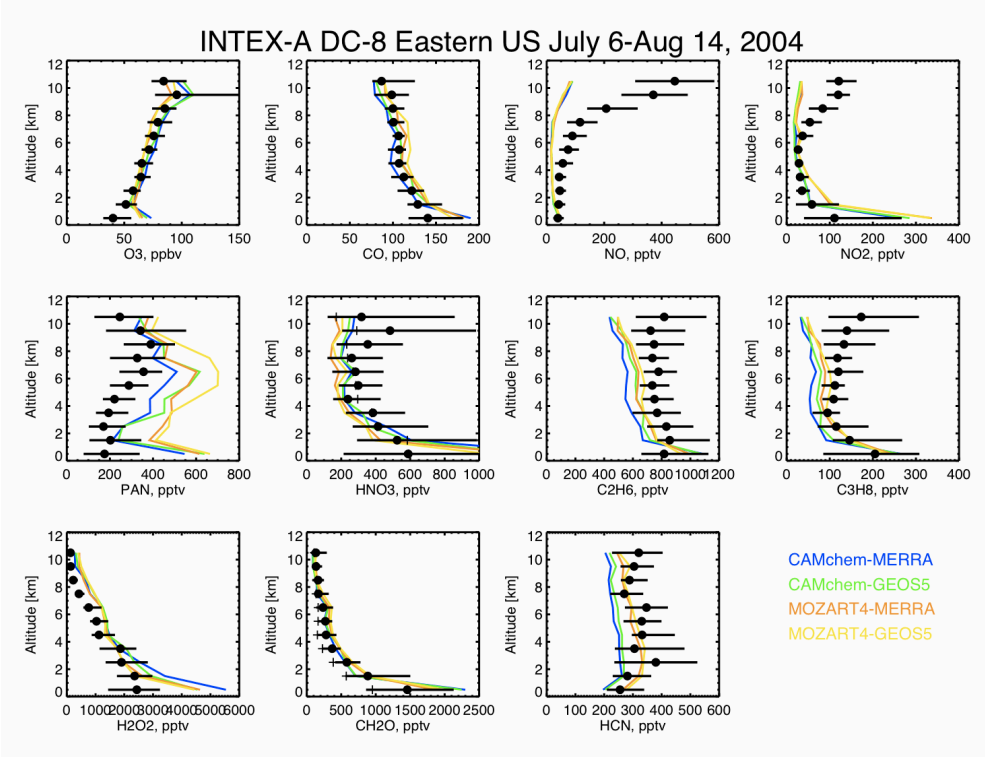

Fig. 6b. Same as Fig. 6a but for INTEX-A Eastern US.

GMDD
4, 2199–2278, 2011

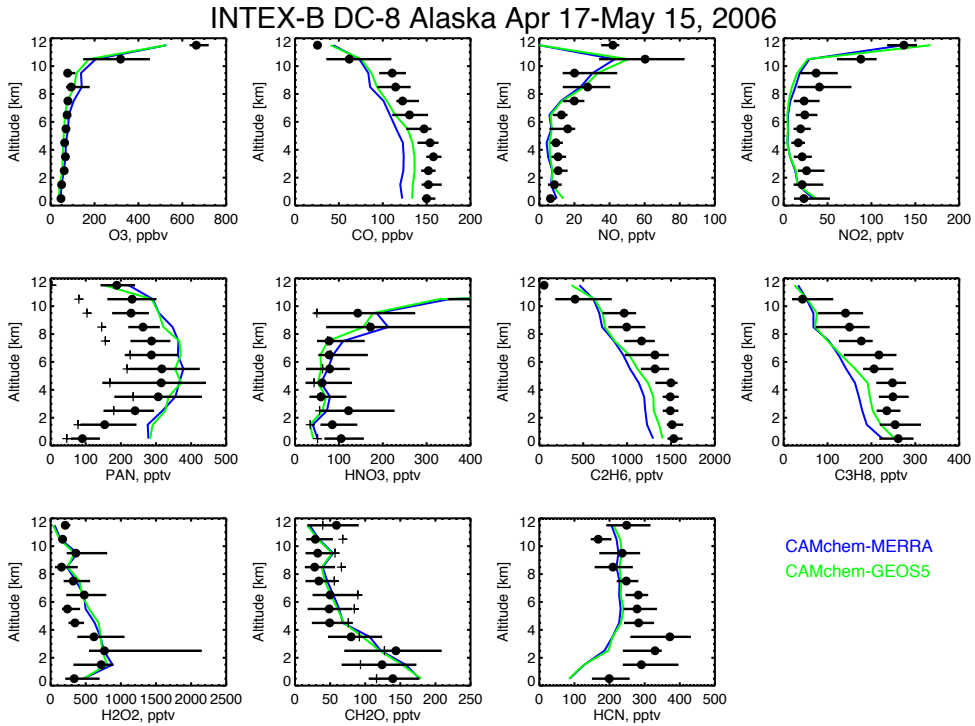

Fig. 6c. Same as Fig. 6a but for INTEX-B Alaska observations.

GMDD
4, 2199–2278, 2011

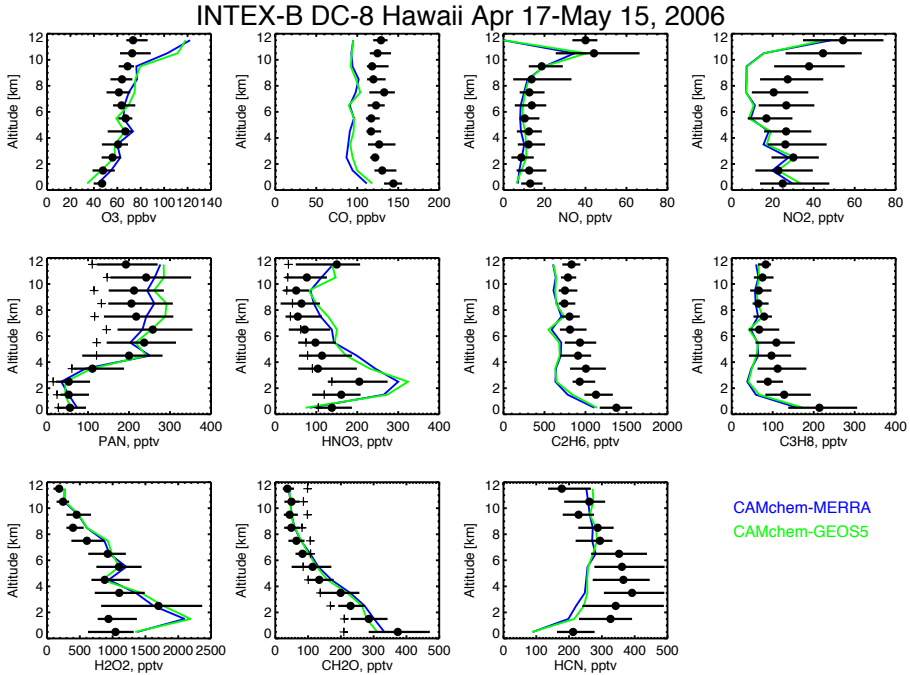

Fig. 6d. Same as Fig. 6a but for INTEX-B Hawaii observations.

GMDD
4, 2199–2278, 2011

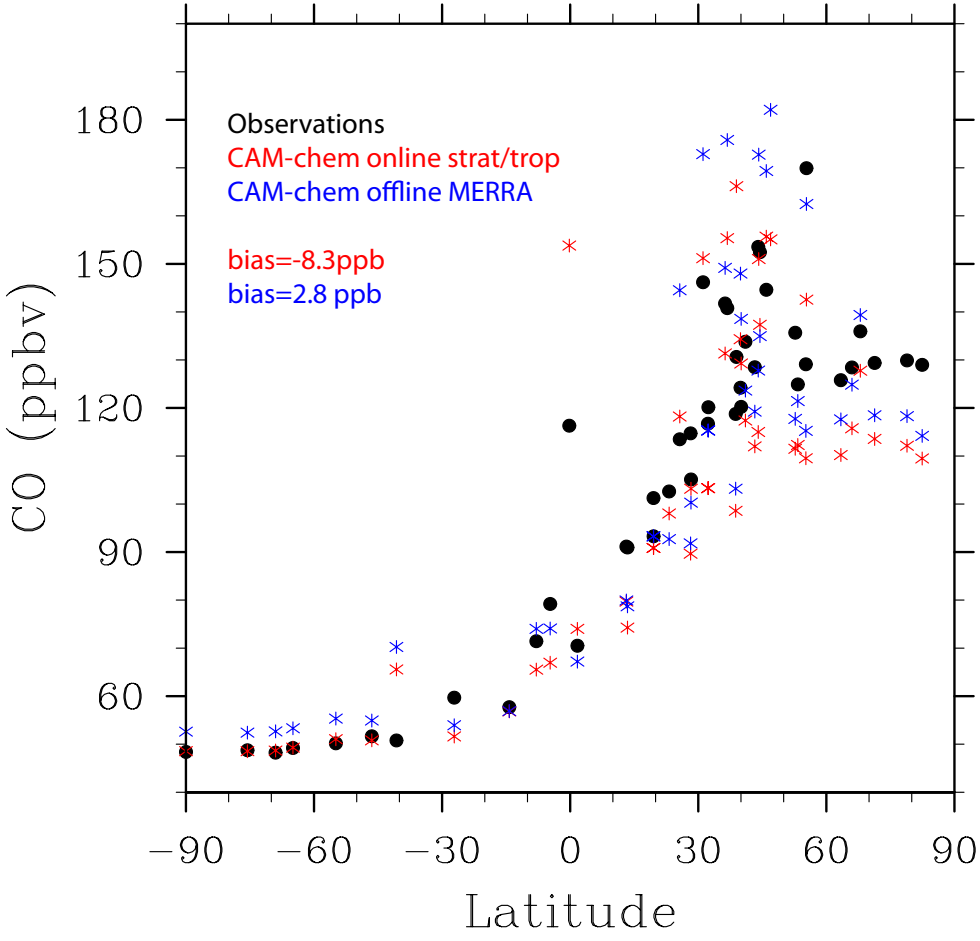

Fig. 7a. Comparison of the annual mean surface mixing ratio of CO to CMDL observations.

GMDD
4, 2199–2278, 2011

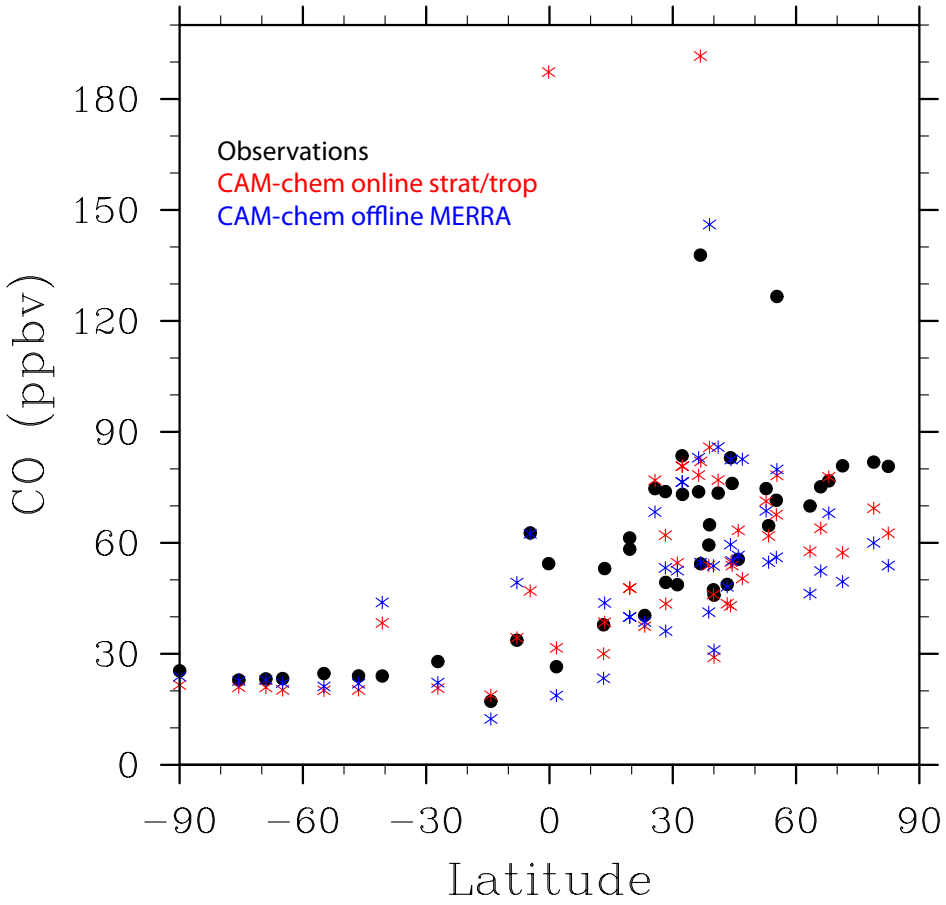

Fig. 7b. Comparison of the mean annual cycle (maximum minus minimum) of surface CO mixing ratio.

GMDD
4, 2199–2278, 2011

CAM-chem description and evaluation

J.-F. Lamarque et al.

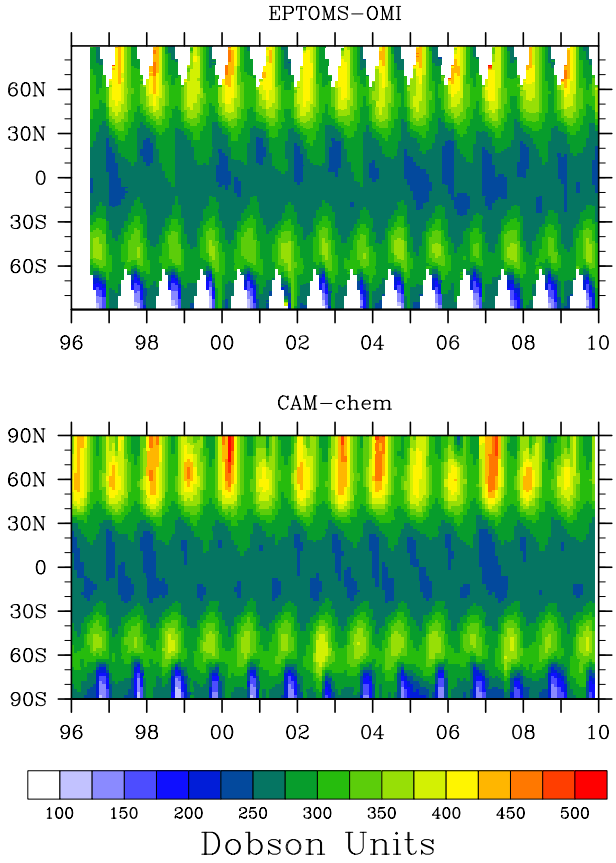

Fig. 8. Time evolution of zonally and monthly-averaged total ozone column (in Dobson Units) from the TOMS instruments (EP-TOMS and OMI-TOMS, top) and online stratosphere-troposphere (bottom).

GMDD
4, 2199–2278, 2011

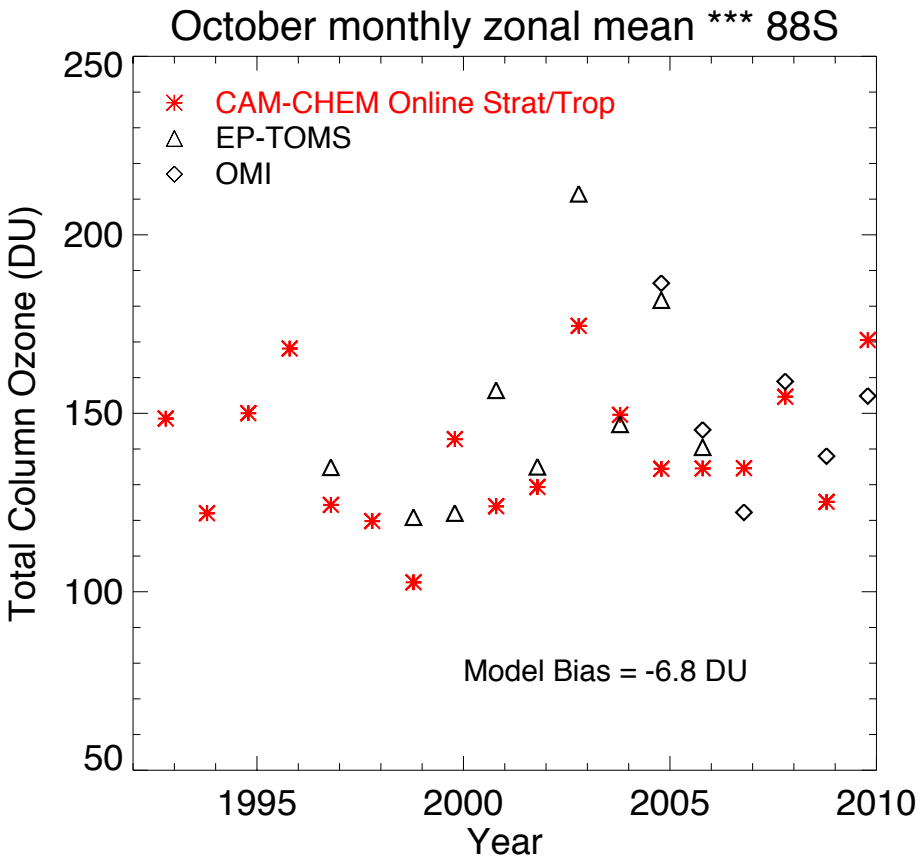

Fig. 9a. Same as Fig. 9a but for 88° S.

GMDD
4, 2199–2278, 2011

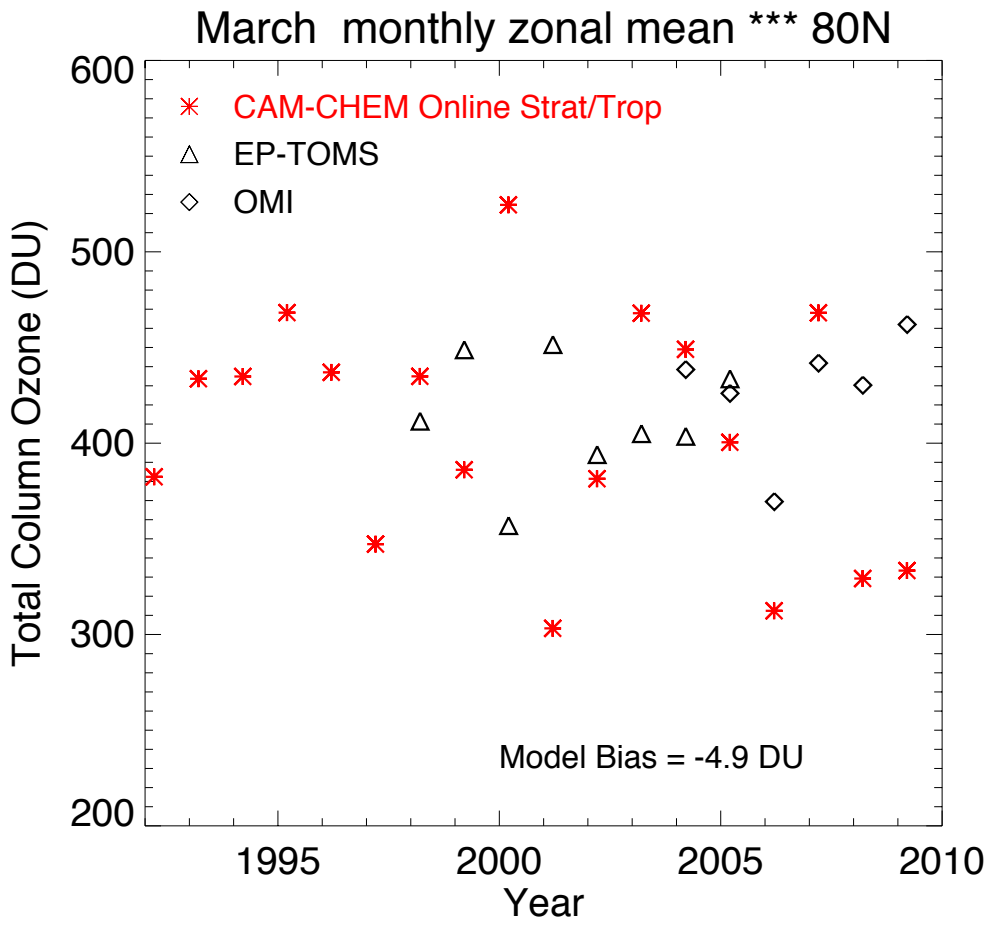

Fig. 9b. Timeseries of March total ozone column at 80° N.

GMDD
4, 2199–2278, 2011

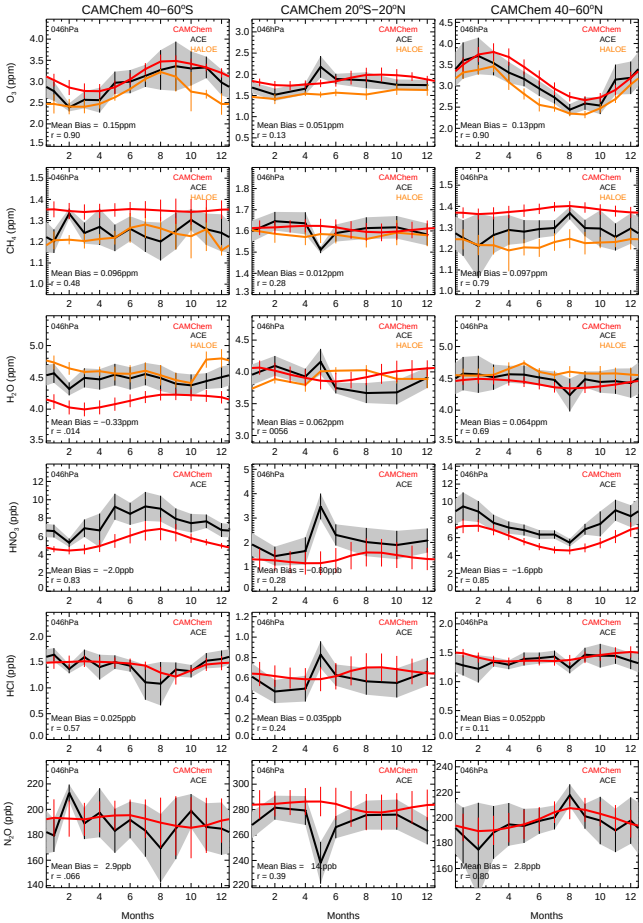

Fig. 10a. Comparison with HALOE and ACE mean seasonal cycle at 46 hPa for 3 latitudinal bands (40 S–60 S, left column; 20 S–20 N, center column; 40 N–60 N; right column).

GMDD
4, 2199–2278, 2011

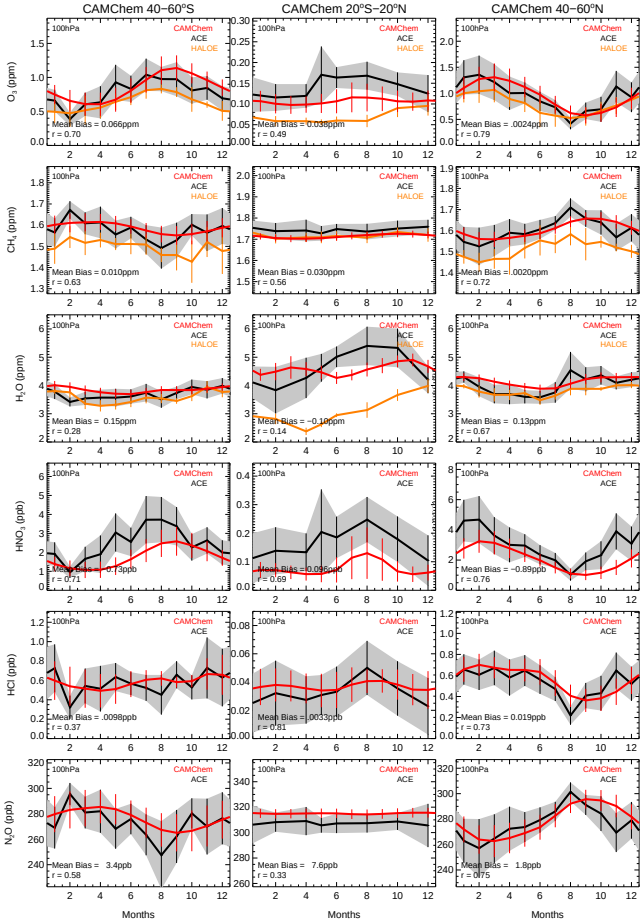

Fig. 10b. Same as Fig. 10a but for 100 hPa.

GMDD
4, 2199–2278, 2011

CAM-chem description and evaluation

J.-F. Lamarque et al.

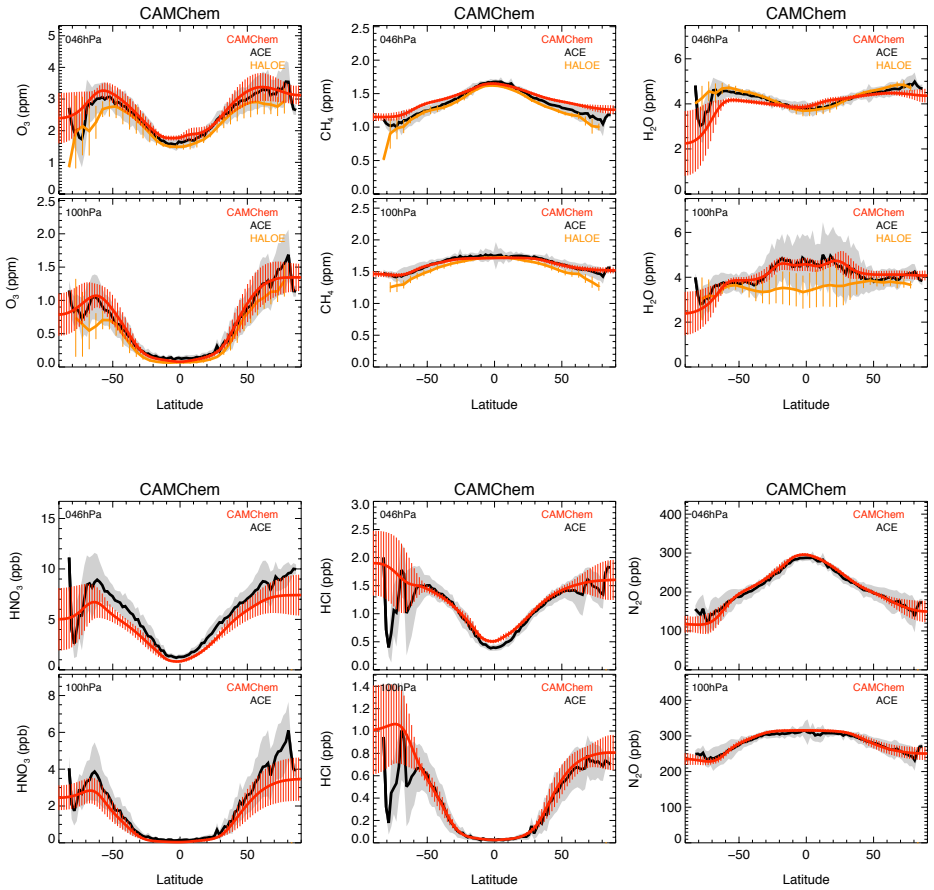

Fig. 11. Latitudinal distribution of the zonally-averaged annual mean modeled and observed (ACE) of several species at 46 and 100 hPa.

GMDD
4, 2199–2278, 2011

CAM-chem description and evaluation

J.-F. Lamarque et al.

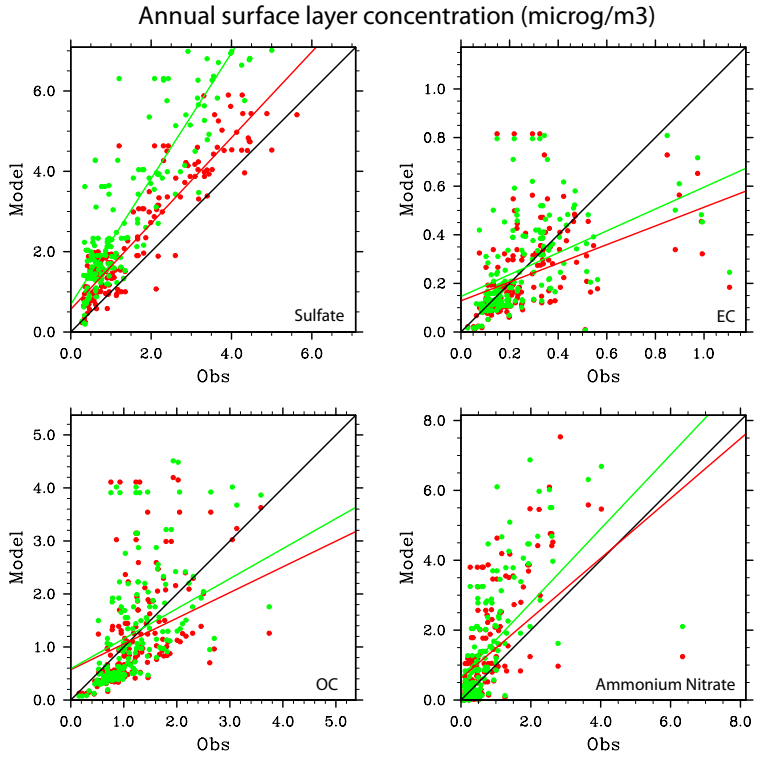

Fig. 12. Linear correlation between observed (IMPROVE sites, black line) and modeled (interpolated to observation sites) annual surface concentrations of aerosols (sulfate, top left; elemental carbon, top right, organic carbon, bottom left, ammonium nitrate, bottom right). The simulation results shown here are for the online stratosphere-troposphere (red) and the GEOS5 simulation (green).

GMDD
4, 2199–2278, 2011

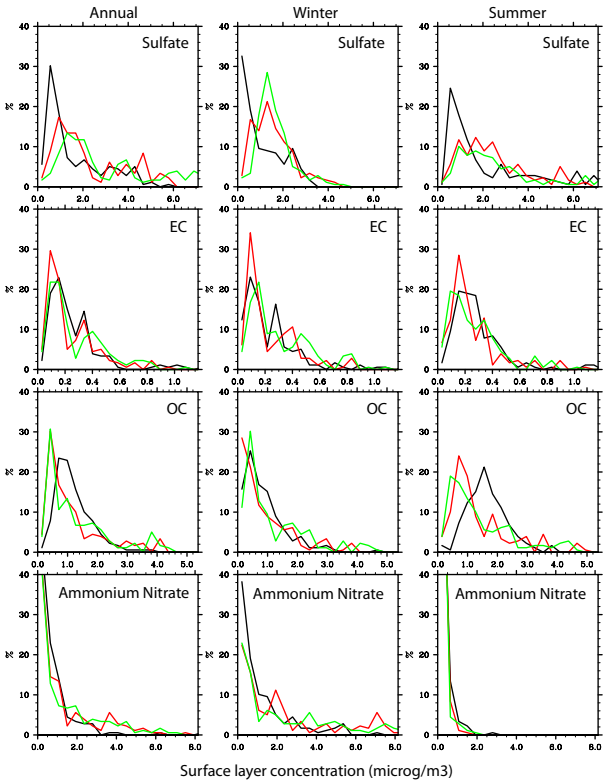

Fig. 13. Probability density function of observed (IMPROVE sites, black line) and modeled (interpolated to observation sites) aerosol surface concentration (sulfate, top row; elemental carbon, second row; organic carbon, third row; ammonium nitrate, bottom row). The simulation results shown here are for the online stratosphere-troposphere (red) and the GEOS5 simulation (green). Analysis is shown for annual (left column), winter (December-January-February, center column) and summer (June-July-August, right column).

GMDD
4, 2199–2278, 2011